Chemico-Biological Interactions 344 (2021) 109530

Contents lists available at ScienceDirect

Chemico-Biological Interactions

journal homepage: www.elsevier.com/locate/chembioint

Research paper

Design, synthesis, and antitumor activity of PLGA nanoparticles incorporating a discovered benzimidazole derivative as EZH2 inhibitor

Hoda A. Elkot [a], Ibrahim Ragab [a], Noha M. Saleh [b,*], Mohamed N. Amin [c], Sara T. Al-Rashood [d], Shahenda M. El-Messery [e], Ghada S. Hassan [f,**]

[a] Faculty of Pharmacy, Mansoura University, P.O. Box 35516, Mansoura, Egypt
[b] Department of Pharmaceutics, Faculty of Pharmacy, Mansoura University, P.O. Box 35516, Mansoura, Egypt
[c] Department of Biochemistry, Faculty of Pharmacy, Mansoura University, P.O. Box 35516, Mansoura, Egypt
[d] Department of Pharmaceutical Chemistry, College of Pharmacy, King Saud University, Riyadh, 11451, Saudi Arabia
[e] Department of Pharmaceutical Organic Chemistry, Faculty of Pharmacy, Mansoura University, P.O. Box 35516, Mansoura, Egypt
[f] Department of Medicinal Chemistry, Faculty of Pharmacy, Mansoura University, P.O. Box 35516, Mansoura, Egypt

ARTICLE INFO

Keywords:
Synthesis
EZH2 inhibitor
PLGA
Nanoparticles
Antitumor activity
EpCAM

ABSTRACT

Purpose: Targeting enhancer of zeste homolog 2 (EZH2) can represent a hopeful strategy for oncotherapy. Also, the use of PLGA-based nanoparticles as a novel and rate-controlling carrier system was of our concern.
Methods: Benzimidazole derivatives were synthesized, and their structures were clarified. *In vitro* antitumor activity was evaluated. Then, a modeling study was performed to investigate the ability of the most active compounds to recognize EZH2 active sites. Compound **30** (Drug) was selected to conduct pre-formulation studies and then it was incorporated into polymeric PLGA nanoparticles (NPs). NPs were then fully characterized to select an optimized formula (NP_4) that subjected to further evaluation regarding antitumor activity and protein expression levels of EZH2 and EpCAM.
Results: The results showed the antitumor activity of some synthesized derivatives. Docking outcomes demonstrated that Compound **30** was able to identify EZH2 active sites. NP_4 exhibited promising findings and proved to keep the antitumor activity of Compound **30**. HEPG-2 was the most sensitive for both Drug and NP_4. Protein analysis indicated that Drug and NP_4 had targeted EZH2 and the downstream signaling pathway leading to the decline of EpCAM expression.
Conclusions: Targeting EZH2 by Compound **30** has potential use in the treatment of cancer especially hepatocellular carcinoma.

1. Introduction

Epigenetic mechanisms are vital for the ordinary growth and maintenance of different gene expression patterns. The failure to properly maintain such heritable epigenetic characters can cause undesirable activation or inhibition of various gene expressions which in turn end with the induction of several diseases. It has been realized that epigenetic abnormalities are involved in the initiation and progression of cancer [1]. Among various pathways, epigenetic changes such as histone modifications by covalent or noncovalent mechanisms and DNA methylation have been verified as promising approaches for oncotherapy [2]. Polycomb repressive complex 2 (PRC2) is accountable for di- or trimethylation of lysine 27 in histone H3 (H3K27me3). The trimethylation process results in a repressive chromatin environment. Therefore, PRC2 has a vital role in silencing gene expression. Enhancer of zeste homolog 2 (EZH2) is a histone-lysine N-methyl transferase enzyme that represents a subunit of PRC2 [3]. Moreover, EZH2 can function independently of the other PRC2 subunits, methylating non-histone proteins [4]. EZH2 over activation is linked to overexpression of epithelial cell adhesion molecule (EpCAM) expressing cancer cells. EpCAM + cells are usually referred to as cancer stem cells, which contribute to tumor malignancy and resistance to chemo/radiotherapy [5]. An association has been well documented between overexpression of EZH2 and aggressiveness of breast cancer, prostate cancer, and especially hepatocellular carcinoma (HCC) [6]. EZH2 affects the expression of very

* Corresponding author.
** Corresponding author.
E-mail address: nunu_ramy@yahoo.com (N.M. Saleh).

https://doi.org/10.1016/j.cbi.2021.109530
Received 22 December 2020; Received in revised form 16 May 2021; Accepted 19 May 2021
Available online 23 May 2021

Abbreviations

Drug	Compound **30**
DIW	Deionized water
DLS	Dynamic Light Scattering
DSC	Differential Scanning Calorimetry
EE%	Encapsulation efficiency
EpCAM	Epithelial cell adhesion molecule
EPR	Enhanced permeation and retention effect
EZH2	Enhancer of zeste homolog 2
FBS	Fetal Bovine serum
FT-IR	Fourier Transform Infrared Spectroscopy
H3K27me3	Trimethylation of lysine 27 in histone H3
HEPG-2	Hepatocellular carcinoma
HLB	Hydrophilic lipophilic balance
$K_{o/w}$	Octanol-water partition coefficient
LC%	Loading capacity
MCF-7	Breast cancer
MTT	3-(4,5-dimethylthiazol-2-yl)-2,5-diphenyl tetrazolium bromide
NPs	Polymeric nanoparticles
$PB_{7.4}/MeOH_{20}$	Phosphate buffer pH 7.4 containing 20% v/v methanol
PBS	Phosphate buffer saline
PC-3	Prostate cancer
PDI	Polydispersity index
PLGA	Poly(D, L-lactide-co-glycolide)
PRC2	Polycomb repressive complex 2
PVA	Polyvinyl alcohol
TEM	Transmission electron microscopy
T_M	Melting points
Y%	Percent yield
Z-average	Average size
ζ	Zeta potential

important tumor suppressor genes such as SNF5 leading to its suppression. Hence, EZH2 is considered a talented therapeutic target for the treatment of hypermethylation-related cancers [7].

Benzimidazole is a central heterocyclic compound and one of the power structures found in a large number of natural products [8]. The heterocyclic nucleus of benzimidazole is considered a "Master Key" in medicinal chemistry. For FDA-approved pharmaceutical drugs, this nucleus is found to be among the top five most common five-membered aromatic nitrogen heterocycles. Several benzimidazole derivatives bearing various substitutions at the C-2 position are widely distributed in nature and possess versatile biological activities. By extensive bioactivities such as anti-protozoal, anti-microbial, antioxidant, analgesic, anti-inflammatory, anti-hypertensive, and anticancer activity, benzimidazole derivatives have an essential role in drug discovery. Benzimidazoles are considered important pharmacophores of cancer research due to wide anticancer capacities with multiple mechanisms. Their anticancer selectivity is contingent on the substitution of the benzimidazole nucleus to provide a track for the development of novel highly effective and target-specific benzimidazole-based anticancer drugs. Hence, benzimidazole derivatives have attracted our attention in this study and we had planned to synthesize a series of new benzimidazole derivatives [9]. The synthesized molecules with promising activities were planned to be incorporated into proper drug delivery systems. Classical drug delivery involves frequent dosing, which usually results in that a major part of the drug tends to be released rapidly after the administration. Such a situation could cause oscillations of drug levels between the side effects level and the minimum effective level with alternating periods of toxicity and ineffectiveness [10]. Hence, controlled drug delivery could be suggested as a strategy to overcome the drawbacks of the conventional one. Controlling the release of drugs can be accomplished by combining appropriate carrier materials with active agents to improve the pattern of drug release, the systemic circulation time, as well as the site drug delivery i.e. pharmacokinetics and pharmacodynamics [11].

Currently, scientists have explored the field of nanotechnology to develop a proper drug carrier system for the effective and controlled delivery of loaded drugs to cancer cells. Due to their extraordinary physicochemical properties, nanomaterials such as nanoparticles; nanocapsules or nanospheres, nanofibers, nanotubes, and nanovesicles realize successful carrier matrices of many drugs [10]. Polymeric nanoparticles (NPs) can be applied to deliver a drug in a rate-controlled and occasionally targeted manner [12]. NPs can permeate through biological barriers due to their reduced size associated with high surface area [13]. The biodistribution of NPs enriches their cellular uptake and improves the drug concentration in tissues. Regularly solid tumors are concealed with a leaky vasculature that drives leakage of NPs from the vasculature through these permeable endothelial tissues to preferentially accumulate in the solid tumors. This phenomenon is called enhanced permeation and retention effect (EPR) and it is useful to promote passive targeting of the chemotherapeutic agent to tumor cells [14]. Hence, tumor tissue by EPR is more permeable owing to the wide fenestrations of the angiogenic vasculature. Besides, NPs are more retained in tumor regions due to a lack of lymphatic around them. Such a situation reducing the exposure of healthy cells to chemotherapeutic drugs [15].

Specific attention has been lately focused on polymeric NPs prepared of several smart biodegradable and biocompatible polymers such as Poly (D, L-lactide-co-glycolide) (PLGA). PLGA-based NPs of many drugs are currently holding FDA approval for several therapeutic applications [16]. PLGA is broadly used to sustain the release of many drugs, enhance the *in vivo* oral bioavailability and therapeutic efficacy [17]. Additionally, PLGA can protect drugs from early degradation and hepatic pass metabolism. The release pattern and rate of a drug could be planned by augmenting particle size, surface charge, morphology, and loading efficiency of PLGA-based NPs [18].

In light of the above details, the present study focused on discovering a benzimidazole-based epigenetic regulator as antagonists of EZH2. Also, their antitumor activity and selectivity were aimed to be explored. Besides, we aimed to enhance the physicochemical properties of these EZH2 inhibitors via incorporation in novel nanocarrier systems based on PLGA NPs. Keeping antitumor activity after incorporation of an EZH2 inhibitor in NPs was of our concern.

2. Experimental

2.1. Materials

PLGA (Purasorb PDLGA®5010, MWt 153 KDa, Purac Biomaterials, Holland), Tween 20 (Polyoxyethylene(20) sorbitan monolaurate, LOBA Chemie Pvt. Ltd., India), Polyvinyl alcohol (PVA, MWt 14 KDa, BDH, USA), RPMI-1640 medium and DMEM-high glucose medium (Lonza, UK), MTT [3-(4,5-dimethylthiazol-2-yl)-2,5-diphenyl tetrazolium bromide] (Serva, Heidelberg, Germany), dimethylsulfoxide (DMSO, Sigma-Aldrich, St. Louis, USA), Fetal Bovine Serum (FBS, Gibco, UK), Methanol and Acetone (El-Nasr Pharmaceutical Chemicals Co., ADWIC, Cairo, Egypt). EZH2 protein ELISA kit (ab264632, Abcam, Cambridge, UK), EpCAM protein ELISA kit (LS-F7278, LSBio, Seattle, WA). All fine reagents and chemicals were obtained from Aldrich Chemicals Co., USA.

2.2. Synthesis of new benzimidazole derivatives

New benzimidazole compounds were synthesized, their melting points (T_M, °C) were determined (Mettler FP 80 melting point apparatus, Mettler, Manchester, UK) and uncorrected. C, H, and N of all compounds were analyzed, and they were found to agree with the suggested structures within ±0.4% of the theoretical values. ^{1}H, ^{13}C NMR of the synthesized compounds were recorded (JOEL 500 MHz FT spectrometer, Japan) and chemical shifts were expressed in δ ppm concerning TMS. On pre-coated silica gel (0.25 mm) GF_{254} plates (Merck, Germany), thin-layer chromatography was performed, and the compounds were detected under a UV lamp at 254 nm. Silica gel with 60–230 mesh was applied for routine separations of column chromatography.

2.2.1. Synthesis of 5,6-(un) substituted-1H-benzo[d]imidazole-2-thiols (4–6)

An alkaline solution of a mixture of diaminobenzene derivative (**1-3**) (0.01 mol) and carbon disulfide (2 ml), potassium hydroxide (0.4 g, 0.01 mol) in (30 ml) methanol has been prepared, refluxed overnight. The obtained solution was evaporated under reduced pressure, and the residue obtained was washed with water, extracted with chloroform. Then, the organic layer was separated and dried over anhydrous sodium sulfate to obtain the required compounds.

*2.2.1.1. 1H-benzo[d]imidazole-2-thiol **(4)***. Yield 85.6%, ^{1}H NMR (500 MHz, DMSO-d_6) δ 7.09 (d, 2H, J = 8.0 Hz, Ar–H), 7.21 (t, 2H, J = 8.5 Hz, Ar–H), 9.32 (s, 1H, NH), 10.39 (s, 1H, SH). Elemental Analysis: Calcd: C, 55.98; H, 4.03; N, 18.65; S, 21.35. Found: C, 56.15; H, 3.99; N, 18.79; S, 21.66. **MS** *m/z* (%): 150.0 (15.4, M^+).

*2.2.1.2. 5,6-dimethyl-1H-benzo[d]imidazole-2-thiol **(5)***. Yield 88.5%, ^{1}H NMR (500 MHz, DMSO-d_6) δ 1.52 (s, 6H, CH_3), 7.51 (s, 2H, Ar–H), 9.61 (s, 1H, NH), 11.61 (s, 1H, SH). Elemental Analysis: Calcd: C, 60.64; H, 5.65; N, 15.72; S, 17.99. Found: C, 60.74; H, 5.48; N, 16.10; S, 17.53. **MS** *m/z* (%): 178.2 (12.3, M^+).

*2.2.1.3. 5,6-dichloro-1H-benzo[d]imidazole-2-thiol **(6)***. Yield 87.3%, ^{1}H NMR (500 MHz, DMSO-d_6) δ 7.94 (s, 2H, Ar–H), 9.51 (s, 1H, NH), 10.99 (s, 1H, SH). Elemental Analysis: Calcd: C, 38.38; H, 1.84; N, 12.79; S, 14.63. Found: C, 38.61; H, 1.72; N, 12.94; S, 15.08. **MS** *m/z* (%): 218.0 (21.3, M^+).

2.2.2. Synthesis of 2-(methylthio)-5,6-(un) substituted-1H-benzo[d] imidazoles (7–9)

(0.01 mol) of compounds **4-6**, was stirred with methyl iodide (10 ml), anhydrous potassium carbonate (1 g) in 50 ml acetone for 24 h. The resultant solution was then evaporated under vacuum and the obtained residue was crystallized from aqueous ethanol to obtain the mentioned derivatives in reasonable yields.

*2.2.2.1. 2-(Methylthio)-1H-benzo[d]imidazole **(7)***. Yield 63.4%, ^{1}H NM R (500 MHz, DMSO-d_6) δ 1.95 (s, 3H, CH_3), 7.12 (d, 2H, J = 7.5 Hz, Ar–H), 7.25 (t, 2H, J = 8.5 Hz, Ar–H), 10.42 (s, 1H, NH). Elemental Analysis: Calcd: C, 58.51; H, 4.91; N, 17.06; S, 19.52. Found: C, 58.25; H, 4.95; N, 17.26; S, 19.86. **MS** *m/z* (%): 164 (8.4, M^+).

*2.2.2.2. 5,6-Dimethyl-2-(methylthio)-1H-benzo[d]imidazole **(8)***. Yield 5 5.4%, ^{1}H NMR (500 MHz, DMSO-d_6) δ 1.67 (s, 6H, CH_3), 1.99 (s, 3H, CH_3), 7.59 (s, 2H, Ar–H), 9.95 (s, 1H, NH). Elemental Analysis: Calcd: C, 62.47; H, 6.29; N, 14.57; S, 16.67. Found: C, 62.53; H, 6.64; N, 14.32; S, 16.82. **MS** *m/z* (%): 192 (17.0, M^+).

*2.2.2.3. 5,6-Dichloro-2-(methylthio)-1H-benzo[d]imidazole **(9)***. Yield 5 9.4%, ^{1}H NMR (500 MHz, DMSO-d_6) δ 1.95 (s, 3H, CH_3), 8.21 (s, 2H, Ar–H), 10.01 (s, 1H, NH). Elemental Analysis: Calcd: C, 41.22; H, 2.59; N, 12.02; S, 13.75. Found: C, 41.35; H, 2.71; N, 12.89; S, 14.17. **MS** *m/z* (%): 232 (11.8, M^+).

2.2.3. Synthesis of 2-hydrazinyl-5,6-(un) substituted-1H-benzo[d] imidazoles (10–12)

A solution of methylthio-benzoimidazole derivatives **7-9** (0.01 mol) in 10 ml hydrazine hydrate was refluxed for 12 h. The resultant solution was then poured into iced water, extracted with methylene chloride, and finally crystallized from ethanol to produce the desired products in good yields.

*2.2.3.1. 2-Hydrazinyl-1H-benzo[d]imidazole **(10)***. Yield 75.4%, ^{1}H N MR (500 MHz, DMSO-d_6) δ 4.41 (s, 2H, NH<u>NH$_2$</u>), 6.38 (d, 2H, J = 8.0 Hz, Ar–H), 7.10 (t, 2H, J = 7.3 Hz, Ar–H), 7.75 (s, 1H, <u>NH</u>NH$_2$), 10.22 (s, 1H, NH). Elemental Analysis: Calcd: C, 56.74; H, 5.44; N, 37.81. Found: C, 56.91; H, 5.72; N, 38.16. **MS** *m/z* (%): 148 (3.1, M^+).

*2.2.3.2. 2-Hydrazinyl-5,6-dimethyl-1H-benzo[d]imidazole **(11)***. Yield 6 7.2%, ^{1}H NMR (500 MHz, DMSO-d_6) δ 1.73 (s, 6H, CH_3), 4.52 (s, 2H, NH<u>NH$_2$</u>), 7.34 (s, 2H, Ar–H), 8.14 (s, 1H, <u>NH</u>NH$_2$), 10.42 (s, 1H, NH). Elemental Analysis: Calcd: C, 61.34; H, 6.86; N, 31.79. Found: C, 61.92; H, 7.08; N, 32.10. **MS** *m/z* (%): 176 (9.7, M^+).

*2.2.3.3. 5,6-Dichloro-2-hydrazinyl-1H-benzo[d]imidazole **(12)***. Yield 8 0.6%, ^{1}H NMR (500 MHz, DMSO-d_6) δ 4.67 (s, 2H, NH<u>NH$_2$</u>), 7.94 (s, 2H, Ar–H), 9.37 (s, 1H, <u>NH</u>NH$_2$), 10.44 (s,1H, NH). Elemental Analysis: Calcd: C, 38.74; H, 2.79; N, 25.81. Found: C, 39.00; H, 2.94; N, 25.49. **MS** *m/z* (%): 216 (12.4, M^+).

2.2.4. Synthesis of (Z)-5,6-(un) substituted-2-(2-substituted benzylidene) hydrazinyl)-1H-benzo[d]imidazoles (17–28)

A mixture of hydrazinyl derivatives **10-12** (0.01 mol) and the appropriately substituted benzaldehyde (0.01 mol) in 30 ml ethanol with a catalytic amount of acetic acid (1 ml) was refluxed for 8 h. Then, the solvent allowed to evaporate under reduced pressure, and the left residue was crystallized by aqueous ethanol to get the required compounds.

*2.2.4.1. (Z)-2-(2-(4-methoxybenzylidene) hydrazinyl)-1H-benzo[d]imida zole **(17)***. Yield 61.7%, ^{1}H NMR (500 MHz, DMSO-d_6) δ 3.75 (s, 3H, OCH_3), 6.47 (s, 1H, N=CH), 7.32 (d, 2H, J = 8.5 Hz, Ar–H), 7.41 (t, 2H, J = 8.0 Hz, Ar–H), 7.62 (d, 2H, J = 8.0 Hz, Ar–H), 7.69 (d, 2H, J = 7.5 Hz, Ar–H), 9.54 (s, 1H, NH), 10.23 (s, 1H, NH). ^{13}C NMR (125 MHz, DMSO-d_6) δ 55.5, 105.3, 110.7, 111.9, 113.0, 115.4, 119.8, 122.4, 123.9, 125.0, 126.3, 129.9, 133.4, 138.6, 139.3. Elemental Analysis: Calcd: C, 67.65; H, 5.30; N, 21.04. Found: C, 68.02; H, 5.63; N, 21.38. **MS** *m/z* (%): 266 (12.4, M^+).

*2.2.4.2. (Z)-2-(2-(2-chlorobenzylidene) hydrazinyl)-1H-benzo[d]imidazo le **(18)***. Yield 57.3%, ^{1}H NMR (500 MHz, DMSO-d_6) δ 6.73 (s, 1H, N=CH), 7.21–7.25 (m, 4H, Ar–H), 7.62–7.67 (m, 4H, Ar–H), 9.82 (s, 1H, NH), 11.01 (s, 1H, NH). ^{13}C NMR (125 MHz, DMSO-d_6) δ 113.4, 114.7, 116.0, 117.2, 118.9, 122.0, 123.7, 126.4, 129.9, 130.4, 132.6, 136.2, 138.7, 140.9. Elemental Analysis: Calcd: C, 62.11; H, 4.10; N, 20.70. Found: C, 62.17; H, 4.23; N, 20.92. **MS** *m/z* (%): 270 (8.0, M^+).

*2.2.4.3. (Z)-2-(2-(4-chlorobenzylidene) hydrazinyl)-1H-benzo[d]imidazo le **(19)***. Yield 64.9%, ^{1}H NMR (500 MHz, DMSO-d_6) δ 6.26 (s, 1H, N=CH), 7.27 (d, 2H, J = 8.5 Hz, Ar–H), 7.31 (d, 2H, J = 8.0 Hz, Ar–H), 7.35–7.39 (m, 4H, Ar–H), 9.54 (s, 1H, NH), 11.22 (s, 1H, NH). ^{13}C NMR (125 MHz, DMSO-d_6) δ 111.0, 114.6, 114.9, 115.1, 116.7, 118.3, 120.6, 122.7, 123.0, 124.5, 127.7, 129.6, 130.4, 138.1. Elemental Analysis: Calcd: C, 62.11; H, 4.10; N, 20.70. Found: C, 62.21; H, 4.27; N, 21.0. **MS** *m/z* (%): 270 (10.2, M^+).

2.2.4.4. (Z)-2-(2-(4-nitrobenzylidene) hydrazinyl)-1H-benzo[d]imidazole ***(20)***. Yield 56.2%, ^{1}H NMR (500 MHz, DMSO-d_6) δ 6.92 (s, 1H, N═CH), 7.26 (d, 2H, J = 7.5 Hz, Ar–H), 7.38 (t, 2H, J = 8.0 Hz, Ar–H), 7.40 (d, 2H, J = 7.5 Hz, Ar–H), 7.51 (d, 2H, J = 8.5 Hz, Ar–H), 9.43 (s, 1H, NH), 10.28 (s, 1H, NH). ^{13}C NMR (125 MHz, DMSO-d_6) δ 116.2, 118.7, 119.1, 119.9, 121.0, 122.5, 123.7, 125.8, 127.9, 128.8, 129.4, 133.1, 135.6, 138.0 Elemental Analysis: Calcd: C, 59.78; H, 3.94; N, 24.90. Found: C, 59.99; H, 4.02; N, 25.01. **MS** *m/z* (%): 281 (36.2, M^+).

2.2.4.5. (Z)-2-(2-(4-methoxybenzylidene) hydrazinyl)-5,6-dimethyl-1H-benzo[d]imidazole ***(21)***. Yield 75.8%, ^{1}H NMR (500 MHz, DMSO-d_6) δ 1.62 (s, 6H, 2CH_3), 3.81 (s, 3H, OCH_3), 6.82 (s, 1H, N═CH), 7.54 (s, 2H, Ar–H), 7.71 (d, 2H, J = 8.5 Hz, Ar–H), 7.75 (d, 2H, J = 8.0 Hz, Ar–H), 9.87 (s, 1H, NH), 11.00 (s, 1H, NH). ^{13}C NMR (125 MHz, DMSO-d_6) δ 18.5, 19.2, 55.5, 115.2, 116.4, 118.9, 120.0, 122.4, 124.1, 127.6, 128.1, 130.0, 132.5, 135.5, 137.8, 138.4, 139.2. Elemental Analysis: Calcd: C, 69.37; H, 6.16; N, 19.03. Found: C, 69.42; H, 6.45; N, 19.31. **MS** *m/z* (%): 294 (8.2, M^+).

2.2.4.6. (Z)-2-(2-(2-chlorobenzylidene) hydrazinyl)-5,6-dimethyl-1H-benzo[d]imidazole ***(22)***. Yield 64.1%, ^{1}H NMR (500 MHz, DMSO-d_6) δ 1.56 (s, 6H, 2CH_3), 6.91 (s, 1H, N═CH), 7.27 (s, 2H, Ar–H), 7.53 (m, 4H, Ar–H), 10.04 (s, 1H, NH), 10.99 (s, 1H, NH). ^{13}C NMR (125 MHz, DMSO-d_6) δ 20.1, 21.3, 115.4, 117.4, 118.1, 120.3, 121.0, 122.7, 125.9, 127.4, 129.4, 131.0, 133.4, 135.6, 137.1, 139.7 Elemental Analysis: Calcd: C, 64.32; H, 5.06; N, 18.75. Found: C, 64.71; H, 5.19; N, 19.09. **MS** *m/z* (%): 298 (17.4, M^+).

2.2.4.7. (Z)-2-(2-(4-chlorobenzylidene) hydrazinyl)-5,6-dimethyl-1H-benzo[d]imidazole ***(23)***. Yield 69.9%, ^{1}H NMR (500 MHz, DMSO-d_6) δ 1.53 (s, 6H, 2CH_3), 7.10 (s, 1H, N═CH), 7.31 (s, 2H, Ar–H), 7.69 (d, 2H, J = 7.5 Hz, Ar–H), 7.74 (d, 2H, J = 8.0 Hz, Ar–H), 10.22 (s, 1H, NH), 11.34 (s, 1H, NH). Elemental Analysis: Calcd: C, 64.32; H, 5.06; N, 18.75. Found: C, 64.95; H, 5.24; N, 19.17. **MS** *m/z* (%): 298 (16.4, M^+).

2.2.4.8. (Z)-5,6-dimethyl-2-(2-(4-nitrobenzylidene) hydrazinyl)-1H-benzo [d]imidazole ***(24)***. Yield 77.3%, ^{1}H NMR (500 MHz, DMSO-d_6) δ 1.49 (s, 6H, 2CH_3), 6.86 (s, 1H, N═CH), 7.37 (s, 2H, Ar–H), 7.59 (m, 4H, Ar–H), 9.99 (s, 1H, NH), 11.01 (s, 1H, NH). ^{13}C NMR (125 MHz, DMSO-d_6) δ 19.8, 21.3, 115.7, 117.9, 118.0, 119.9, 121.4, 122.5, 123.6, 125.0, 127.0, 127.9, 129.6, 133.6, 135.4, 137.4. **MS** *m/z* (%): 309 (21.0, M^+).

2.2.4.9. (Z)-5,6-Dichloro-2-(2-(4-methoxybenzylidene) hydrazinyl)-1H-benzo[d]imidazole ***(25)***. Yield 65.3%, ^{1}H NMR (500 MHz, DMSO-d_6) δ 3.71 (s, 3H, OCH_3), 6.40 (s, 1H, N═CH), 7.13 (s, 1H, Ar–H), 7.26 (s, 1H, Ar–H), 7.45 (d, 2H, J = 7.9 Hz, Ar–H), 7.52 (d, 2H, J = 8.0 Hz, Ar–H), 9.91 (s, 1H, NH), 10.00 (s, 1H, NH). ^{13}C NMR (125 MHz, DMSO-d_6) δ 55.5, 104.5, 105.6, 110.1, 111.6, 112.2, 114.8, 117.3, 120.4, 122.6, 123.7, 128.4, 130.6, 133.0. Elemental Analysis: Calcd: C, 53.75; H, 3.61; N, 16.72. Found: C, 54.01; H, 3.82; N, 16.99. **MS** *m/z* (%): 334 (17.4, M^+).

2.2.4.10. (Z)-5,6-Dichloro-2-(2-(2-chlorobenzylidene) hydrazinyl)-1H-benzo[d]imidazole ***(26)***. Yield 52.3%, ^{1}H NMR (500 MHz, DMSO-d_6) δ 6.35 (s, 1H, N═CH), 7.13 (s, 1H, Ar–H), 7.27 (s, 1H, Ar–H), 7.37–7.42 (m, 4H, Ar–H), 9.46 (s, 1H, NH), 10.54 (s, 1H, NH). ^{13}C NMR (125 MHz, DMSO-d_6) δ 115.2, 116.4, 120.9, 122.6, 123.0, 124.6, 127.0, 129.3, 131.0, 132.7, 133.9, 136.1, 137.5, 139.0. Elemental Analysis: Calcd: C, 49.51; H, 2.67; N, 16.50. Found: C, 49.82; H, 2.94; N, 16.73. **MS** *m/z* (%): 338 (24.6, M^+).

2.2.4.11. (Z)-5,6-Dichloro-2-(2-(4-chlorobenzylidene) hydrazinyl)-1H-benzo[d]imidazole ***(27)***. Yield 64.3%, ^{1}H NMR (500 MHz, DMSO-d_6) δ 7.01 (s, 1H, N═CH), 7.39 (s, 2H, Ar–H), 7.45 (d, 2H, J = 8.0 Hz, Ar–H), 7.56 (d, 2H, J = 8.0 Hz, Ar–H), 9.88 (s, 1H, NH), 11.06 (s, 1H, NH). ^{13}C NMR (125 MHz, DMSO-d_6) δ 115.3, 116.7, 120.2, 122.6, 123.7, 124.1, 125.9, 127.2, 129.4, 131.7, 133.3, 136.7. 138.0. Elemental Analysis: Calcd: C, 49.51; H, 2.67; N, 16.50. Found: C, 49.91; H, 2.01; N, 16.91. **MS** *m/z* (%): 338 (11.0, M^+).

2.2.4.12. (Z)-5,6-Dichloro-2-(2-(4-nitrobenzylidene) hydrazinyl)-1H-benzo[d]imidazole ***(28)***. Yield 71.3%, ^{1}H NMR (500 MHz, DMSO-d_6) δ 6.84 (s, 1H, N═CH), 7.24 (s, 2H, Ar–H), 7.50 (m, 4H, Ar–H), 10.24 (s, 1H, NH), 10.94 (s, 1H, NH). Elemental Analysis: Calcd: C, 48.02; H, 2.59; N, 20.00 Found: C, 48.51; H, 2.91; N, 20.34. **MS** *m/z* (%): 349 (18.7, M^+).

2.2.5. General procedure for the synthesis of 3-((5,6-(un) substituted)-1H-benzo[d]imidazole-2-yl) amino)-2-(substituted phenyl)-1,3-thiazinan-4-ones (30–41)

Derivatives **17-28** (0.01 mol) were dissolved in 30 ml benzene, then cyclizing agent mercaptopropanoic acid (1 ml) was added and the mixture was refluxed overnight. Then, the solvent was evaporated under reduced pressure and left to obtain final crystals of compounds **30-41**. A little amount of sodium carbonate was dissolved in distilled water and added to the crystals to get rid of the excess mercaptopropanoic acid.

2.2.5.1. 3-((1H-Benzo[d]imidazole-2-yl) amino)-2-(4-methoxyphenyl)-1,3-thiazinan-4-one ***(30)***. Yield 71.5%, ^{1}H NMR (500 MHz, DMSO-d_6) δ 3.70 (s, 3H, OCH_3), 2.73 (t, 2H, J = 1.5 Hz, CH_2), 2.85 (t, 2H, J = 1.5 Hz, CH_2), 4.92 (s, 1H, CH), 7.11 (d, 2H, J = 8.0 Hz, Ar–H), 7.32 (d, 2H, J = 8.0 Hz, Ar–H), 7.45 (t, 2H, J = 8.0 Hz, Ar–H), 7.53 (d, 2H, J = 7.5 Hz, Ar–H), 9.82 (s, 1H, NH), 10.10 (s, 1H, NH). Elemental Analysis: Calcd: C, 61.00; H, 5.12; N, 15.81. Found: C, 61.22; H, 5.17; N, 15.91. **MS** *m/z* (%): 354 (19.7, M^+).

2.2.5.2. 3-((1H-Benzo[d]imidazole-2-yl) amino)-2-(2-chlorophenyl)-1,3-thiazinan-4-one ***(31)***. Yield 66.4%, ^{1}H NMR (500 MHz, DMSO-d_6) δ 2.77 (t, 2H, J = 2.5 Hz, CH_2) 2.93 (t, 2H, J = 2.0 Hz, CH_2), 4.99 (s, 1H, CH), 7.31–7.38 (m, 4H, Ar–H), 7.52–7.60 (m, 4H, Ar–H), 8.57 (s, 1H, NH), 9.93 (s, 1H, NH). ^{13}C NMR (125 MHz, DMSO-d_6) δ 25.4, 28.7, 49.3, 114.8, 115.1, 117.3, 119.0, 120.2, 122.9, 124.7, 126.0, 128.6, 131.0, 133.4, 145.3, 146.3, 159.5. Elemental Analysis: Calcd: C, 56.90; H, 4.21; N, 15.61. Found: C, 57.12; H, 4.43; N, 15.94. **MS** *m/z* (%): 358 (16.3, M^+).

2.2.5.3. 3-((1H-Benzo[d]imidazole-2-yl) amino)-2-(4-chlorophenyl)-1,3-thiazinan-4-one ***(32)***. Yield 73.1%, ^{1}H NMR (500 MHz, DMSO-d_6) δ 2.61 (t, 2H, J = 2.0 Hz, CH_2), 2.80 (t, 2H, J = 2.5 Hz, CH_2), 5.01 (s, 1H, CH), 7.00 (d, 2H, J = 8.5 Hz, Ar–H), 7.38 (d, 2H, J = 8.0 Hz, Ar–H), 7.49–7.53 (m, 4H, Ar–H), 9.24 (s, 1H, NH), 9.84 (s, 1H, NH). ^{13}C NMR (125 MHz, DMSO-d_6) δ 27.3, 27.9, 42.5, 110.5, 113.7, 117.2, 121.0, 122.6, 124.6, 127.1, 130.0, 133.8, 135.4, 141.1, 145.3, 157.2. Elemental Analysis: Calcd: C, 56.90; H, 4.21; N, 15.61. Found: C, 57.03; H, 4.53; N, 15.81. **MS** *m/z* (%): 358 (7.5, M^+).

2.2.5.4. 3-((1H-benzo[d]imidazole-2-yl) amino)-2-(4-nitrophenyl)-1,3-thiazinan-4-one ***(33)***. Yield 75.4%, ^{1}H NMR (500 MHz, DMSO-d_6) δ 2.86 (t, 2H, J = 2.6 Hz, CH_2), 2.89 (t, 2H, J = 2.5 Hz, CH_2), 4.97 (s, 1H, CH), 7.31–7.35 (m, 4H, Ar–H), 7.43–7.48 (m, 4H, Ar–H), 9.02 (s, 1H, NH), 9.37 (s, 1H, NH). Elemental Analysis: Calcd: C, 55.28; H, 4.09; N, 18.96. Found: C, 55.73; H, 4.28; N, 19.34.

2.2.5.5. 3-((5,6-Dimethyl-1H-benzo[d]imidazole-2-yl) amino)-2-(4-methoxyphenyl)-1,3-thiazinan-4-one ***(34)***. Yield 76.2%, ^{1}H NMR (500 MHz, DMSO-d_6) δ 1.51 (s, 3H, CH_3), 1.54 (s, 3H, CH_3), 2.70 (t, 2H, J = 1.0 Hz, CH_2), 2.83 (t, 2H, J = 1.5 Hz, CH_2), 3.75 (s, 3H, OCH_3), 5.11 (s, 1H, CH), 7.24 (s, 2H, Ar–H), 7.36 (d, 2H, J = 8.0 Hz, Ar–H), 7.51 (d, 2H, J = 8.0 Hz, Ar–H), 8.57 (s, 1H, NH), 10.02 (s, 1H, NH). **MS** *m/z* (%): 382 (25.3, M^+).

2.2.5.6. 2-(2-Chlorophenyl)-3-((5,6-dimethyl-1H-benzo[d]imidazole-2-yl) amino)-1,3-thiazinan-4-one ***(35)***. Yield 59.1%, ^{1}H NMR (500 MHz, DMSO-d_6) δ 1.63 (s, 3H, CH_3), 1.71 (s, 3H, CH_3), 2.64 (t, 2H, $J = 2.0$ Hz, CH_2) 2.87 (t, 2H, $J = 2.0$ Hz, CH_2), 4.84 (s, 1H, CH), 7.01 (s, 1H, NH), 7.41–7.46 (m, 4H, Ar–H), 7.53 (s, 1H, Ar–H), 7.61 (s, 1H, Ar–H), 9.97 (s, 1H, NH). ^{13}C NMR (125 MHz, DMSO-d_6) δ 19.1, 20.3, 24.7, 29.0, 47.1, 113.9, 115.2, 117.0, 120.4, 122.4, 123.6, 130.8, 132.6, 158.1. Elemental Analysis: Calcd: C, 58.98; H, 4.95; N, 14.48. Found: C, 29.14; H, 5.21; N, 14.92. **MS** *m/z* (%): 386 (21.0, M^+).

2.2.5.7. 2-(4-Chlorophenyl)-3-((5,6-dimethyl-1H-benzo[d]imidazole-2-yl) amino)-1,3-thiazinan-4-one ***(36)***. Yield 76.3%, ^{1}H NMR (500 MHz, DMSO-d_6) δ 1.68 (s, 3H, CH_3), 1.71 (s, 3H, CH_3), 2.69 (t, 2H, $J = 2.0$ Hz, CH_2), 2.82 (t, 2H, $J = 2.5$ Hz, CH_2), 4.81 (s, 1H, CH), 7.24 (d, 2H, $J = 8.0$ Hz, Ar–H), 7.29 (s, 1H, Ar–H), 7.34 (d, 2H, $J = 8.0$ Hz, Ar–H), 7.36 (s, 1H, Ar–H), 9.61 (s, 1H, NH), 9.93 (s, 1H, NH). Elemental Analysis: Calcd: C, 58.98; H, 4.95; N, 14.48. Found: C, 58.82; H, 5.04; N, 14.73. **MS** *m/z* (%): 386 (23.1, M^+).

2.2.5.8. 3-((5,6-dimethyl-1H-benzo[d]imidazole-2-yl) amino)-2-(4-nitrophenyl)-1,3-thiazinan-4-one ***(37)***. Yield 73.1%, ^{1}H NMR (500 MHz, DMSO-d_6) δ 1.63 (s, 6H, $2CH_3$), 2.81 (t, 2H, $J = 1.5$ Hz, CH_2), 2.92 (t, 2H, $J = 2.5$ Hz, CH_2), 5.11 (s, 1H, CH), 7.16–7.20 (m, 4H, Ar–H), 7.49–7.53 (m, 4H, Ar–H), 8.93 (s, 1H, NH), 10.21 (s, 1H, NH). ^{13}C NMR (125 MHz, DMSO-d_6) δ 15.1, 17.3, 28.4, 30.2, 46.1, 111.5, 113.7, 116.0, 118.2, 121.4, 125.6, 128.0, 128.6, 131.9, 134.2, 139.9, 140.0, 147.2, 157.9. Elemental Analysis: Calcd: C, 57.42; H, 4.82; N, 17.62. Found: C, 57.66; H, 5.13; N, 17.94. **MS** *m/z* (%): 397 (8.6, M^+).

2.2.5.9. 3-((5,6-Dichloro-1H-benzo[d]imidazole-2-yl) amino)-2-(4-methoxyphenyl)-1,3-thiazinan-4-one ***(38)***. Yield 86.4%, ^{1}H NMR (500 MHz, DMSO-d_6) δ 2.75 (t, 2H, $J = 2.0$ Hz, CH_2), 2.82 (t, 2H, $J = 1.5$ Hz, CH_2), 3.72 (s, 3H, OCH_3), 4.68 (s, 1H, CH), 7.24 (d, 2H, $J = 7.5$ Hz, Ar–H), 7.31 (s, 2H, Ar–H), 7.42 (d, 2H, $J = 8.0$ Hz, Ar–H), 8.24 (s, 1H, NH), 9.50 (s, 1H, NH). ^{13}C NMR (125 MHz, DMSO-d_6) δ 26.9, 28.3, 47.0, 112.4, 116.0, 117.4, 120.9, 121.7, 124.1, 126.2, 127.3, 129.0, 130.4, 132.7, 135.6, 138.1, 146.3, 158.4. **MS** *m/z* (%): 422 (12.1, M^+).

2.2.5.10. 2-(2-Chlorophenyl)-3-((5,6-dichloro-1H-benzo[d]imidazole-2-yl) amino)-1,3-thiazinan-4-one ***(39)***. Yield 79.1%, ^{1}H NMR (500 MHz, DMSO-d_6) δ 2.75 (t, 2H, $J = 2.0$ Hz, CH_2), 2.86 (t, 2H, $J = 2.5$ Hz, CH_2), 4.92 (s, 1H, CH), 7.31 (m, 4H, Ar–H), 7.35 (s, 1H, Ar–H), 7.39 (s, 1H, Ar–H), 8.41 (s, 1H, NH), 10.31 (s, 1H, NH). Elemental Analysis: Calcd: C, 47.74; H, 3.06; N, 13.10. Found: C, 47.99; H, 3.27; N, 13.73. **MS** *m/z* (%): 426 (16.2, M^+).

2.2.5.11. 2-(4-Chlorophenyl)-3-((5,6-dichloro-1H-benzo[d]imidazole-2-yl) amino)-1,3-thiazinan-4-one ***(40)***. Yield 66.4%, ^{1}H NMR (500 MHz, DMSO-d_6) δ 2.76–2.79 (m, 4H, $2CH_2$), 4.80 (s, 1H, CH), 7.20–7.25 (m, 4H, Ar–H), 7.49 (s, 2H, Ar–H), 10.05 (s, 1H, NH), 10.47 (s, 1H, NH). ^{13}C NMR (125 MHz, DMSO-d_6) δ 27.4, 29.3, 47.0, 113.7, 114.2, 116.7, 118.0, 119.4, 123.3, 127.2, 129.0, 131.5, 134.8, 136.2, 138.6, 139.2, 159.4. Elemental Analysis: Calcd: C, 47.74; H, 3.06; N, 13.10. Found: C, 47.93; H, 3.24; N, 13.52. **MS** *m/z* (%): 426 (10.2, M^+).

2.2.5.12. 3-((5,6-Dichloro-1H-benzo[d]imidazole-2-yl) amino)-2-(4-nitrophenyl)-1,3-thiazinan-4-one ***(41)***. Yield 69.5%, ^{1}H NMR (500 MHz, DMSO-d_6) δ 2.82–2.90 (m, 4H, $2CH_2$), 5.25 (s, 1H, CH), 7.26–7.30 (m, 4H, Ar–H), 7.51–7.57 (m, 4H, Ar–H), 8.93 (s, 1H, NH), 9.64 (s, 1H, NH). ^{13}C NMR (125 MHz, DMSO-d_6) δ 28.7, 30.7, 45.1, 114.9, 116.1, 118.0, 119.9, 122.4, 125.8, 127.3, 129.1, 130.0, 135.7, 141.6, 158.2. Elemental Analysis: Calcd: C, 46.59; H, 2.99; N, 15.98. Found: C, 46.86; H, 3.12; N, 16.34. **MS** *m/z* (%): 437 (16.8, M^+).

2.3. Screening of in vitro antitumor activity

The synthesized compounds were screened for their antitumor activity versus different cancer cell lines; hepatocellular carcinoma (HEPG-2), breast cancer (MCF-7), and prostate cancer (PC-3). The cell lines were acquired from ATCC via Holding Company for Biological Products and Vaccines (VACSERA), Cairo, Egypt. To serve as a standard anticancer drug, doxorubicin (DOX) was used at serial concentrations ranging from 1.5 to 100 μM (Positive control). The cytotoxic effect was determined using the MTT colorimetric assay. In a medium of RPMI-1640 with 100 U/ml penicillin, 100 μg/ml streptomycin, and 10% FBS, cells were cultured at 37 °C in a 5% CO_2 incubator. At a density of 10^4 cells/well, the cell lines were seeded in a 96-well plate. After incubation, cell lines were treated with serial concentrations of the synthesized compounds that ranged from 1.5 to 100 μM for 24 h. The synthesized compounds were dissolved in DMSO. At the end of the incubation period, cells were subjected to the MTT cell viability assay. Briefly, cells were washed with phosphate buffer saline (PBS), treated with 20 μl of MTT solution (5 mg/ml), and incubated for 4 h at 37 °C. Then, DMSO (100 μl) was added to each well to dissolve the formed purple formazan crystals. The optical densities of wells were determined at 570 nm using a microplate reader (Dynatech, Melville, NY, USA). Experiments were done in triplicates and the viability of non-treated cells (DMSO control) was used to calculate the mean relative viability percentage. Furthermore, the concentration required to kill 50% of cells relative to the control cells was designated as the half-maximal inhibitory concentration (IC_{50}) and it was determined using GraphPad Prism 6.0 (GraphPad Software, USA). Statistical Analysis was done using One-way ANOVA with Tukey post-hock test. Significance was set at $P < 0.05$.

By taking a closer look at the results obtained, it was revealed that the target derivatives **(30-41)** exerted promising activity against the tested cell lines. Among this series, Compounds **30** and **31** were found to be the most active derivative. Hence, these two derivatives were subjected to molecular modeling to investigate their potential interaction with the target protein. Based on the outcomes of the antitumor activity and docking studies, Compound **30** (Drug) had been selected to undergo further evaluations. The MTT cell viability assay against normal human liver cells (THLE-2, VACSERA, Egypt) was performed as described above after 24 h and 72 h incubation to test the effect of Compound **30** against the normal cells. Also, Compound **30** was loaded in different formulations of PLGA-based NPs. The physicochemical evaluation of NPs, which was mentioned later in this study, had directed us to select NP_4 as an optimized formula for further evaluation. Drug and equivalent amounts of NP_4 were prepared at the concentration range of 1.5–100 μM. Their antitumor activities were tested as stated above for 24 h and 72 h of incubation.

2.4. Molecular docking

This section of our study had aimed to perform docking and investigation of the prospective mechanism of action of some of the promising newly synthesized compounds. Three-dimensional structures of some substituted amide benzimidazole derivatives to represent the best EZH2 inhibitors, in their neutral forms, were constructed using Molecular Operating Environment software (MOE of Chemical Computing Group Inc.). A reported reference molecule with a benzimidazole nucleus and selective EZH2 inhibition was used [19]. The lowest energy conformer of new analogs 'global-minima' was docked into the binding pocket of the EZH2 enzyme which is subunit 3 of PRC2 to suggest the mechanism of epigenetic regulation as antitumor activity. The required PDB protein under investigation was obtained from the Protein Data Bank of Brookhaven National Laboratory. Hydrogens were firstly added, followed by the subjection of the enzyme structure to a refinement protocol. The constraints on the enzyme were progressively removed and minimized till the RMSD gradient reached the value of 0.01 kcal/mol Å. Molecular mechanics force field 'AMBER.' Was used for energy minimization.

Energy minimizations (EM) were performed for each benzimidazole derivative using 1000 steps of steepest descent. After that, the conjugate gradient minimization to an RMSD energy gradient of 0.01 kcal/mol Å was acquired. By using a radius of 10.0 Å around MTX, the active site of the enzyme was distinguished. Binding energy was calculated as the difference between the complex energy and the individual energies of the ligand and enzyme. The compounds under docking study were subjected to a flexible alignment experiment using MOE. The builder module of MOE was used to construct the structure of the molecules. Their geometry was enhanced by using the MMFF94 force field. The Lowest energy-aligned conformers were identified and have been used in the docking study.

2.5. Preformulation study

2.5.1. The solubility of Compound 30

The solubility of Compound 30 was determined in deionized water (DIW) and in phosphate buffer pH 7.4 containing 20% v/v methanol ($PB_{7.4}$/$MeOH_{20}$) as solvents. An excess amount of Compound 30 (10 mg) was transferred to screw-capped tubes and 5 mL of solvent were added. Then, the tubes were secured and continuously shaken in a reciprocating water bath (Fisher Scientific, USA) at 37 ± 0.5 °C for 72 h to attain equilibrium. Excess undissolved Compound 30 was removed by centrifugation at 5000 rpm for 30 min. The supernatant was separated, filtered through a 0.45 μm millipore filter, and analyzed spectrophotometrically at 290 nm (λ_{max}) after appropriate dilution (UV-VIS Spectro double beam, Labomed Inc., USA). A pre-determined spectrum of Compound 30 showed that the optimal absorbance peak was at 290 nm. Therefore, 290 nm was used as λ_{max} to construct a standard curve that was found to comply with Beer-Lambert's Law (R^2 = 0.9994). A range of known concentrations was prepared so that the measured absorbance was maintaining values below 1. Triplicates of each solvent were achieved, and the measured absorbance was converted into concentration according to the following equation:

$$Y = 0.05399X + 0.005854$$

Where Y is the absorbance at 290 nm at the corresponding concentration (X).

2.5.2. Octanol-water partition coefficient and log P of Compound 30

$K_{o/w}$ and log P values of Compound 30 were determined using the method reported by Jesus et al. with some modifications [20]. Water and n-octanol were co-saturated with each other by mixing equals amounts of them at 37 ± 0.5 °C for 72 h. Then, the obtained biphasic mixture was transferred to a separating funnel and left for 48 h to allow full separation of the two layers. The octanol-saturated water was pipetted and used to prepare a Compound 30-saturated aqueous solution with a known concentration (C_{Total}). After that, equal amounts of the water-saturated organic phase and Compound 30-saturated aqueous phase were transferred to screw-capped glass tubes that were continuously mixed in a reciprocating water bath at 37 ± 0.5 °C for 72 h to attain equilibrium. The mixture of organic and aqueous layers was then left until complete separation. The concentration of Compound 30 in the aqueous phase was analyzed spectrophotometrically at 290 nm using a pre-constructed calibration curve ($C_{Aqueous}$). $K_{o/w}$ and log P were determined using the following equations [20]:

$$K_{o/w} = \frac{C_{Octanol}}{C_{Aqueous}} = \frac{C_{Total} - C_{Aqueous}}{C_{Aqueous}}$$

$$\log P = Log\ K_{o/w}$$

Predictable values of aqueous solubility and partition coefficient of Compound 30 were also determined using the Swiss ADME web tool (http://www.swissadme.ch) that provides open access to a group of fast predictive models for determination of physicochemical properties and pharmacokinetics [21].

Table 1
Composition and physicochemical properties of the prepared Drug-loaded NPs.

Ingredient % W/V	Formulation code			
	NP_1	NP_2	NP_3	NP_4
PLGA	1	0.6	1	0.6
Compound 30	0.1	0.06	0.1	0.06
PVA	2	2	-	-
T_{20}	-	-	2	2
Item	Evaluation (mean ± SD)			
Z-average	Almost all polymer		252.2 ± 17.4	256.2 ± 4.8
PDI	separated as coarse		0.18 ± 0.05	0.19 ± 0.03
ζ	agglomerates and no		−10.04 ± 3.96	−16.58 ± 4.4
EE%	formation of NPs		14.9 ± 7.41	35.41 ± 5.33
LC%			1.56 ± 0.15	4.15 ± 0.43
Y%			18.14 ± 8.1	46.19 ± 6.72

Z-average, Average size; ***PDI***, polydispersity index; ***ζ***, zeta potential, ***EE%***, encapsulation efficiency; ***LC%***, loading capacity; ***Y%***, percent yield.

2.5.3. Fourier transform infrared spectroscopy (FT-IR)

FT-IR spectroscopy was performed for unprocessed Compound 30, PLGA, the physical binary mixture, and later the formed polymeric NPs; NP_3, and NP_4 at room temperature. Samples were physically mixed with a suitable amount of potassium bromide using a mortar and pestle, compressed using a hydraulic press to a disc, and placed in a diffused reflectance cell (Thermo Fisher Scientific, Inc., Waltham, MA, USA). The spectra of samples were scanned over wave number in a range of 400–4000 cm^{-1}.

2.5.4. Thermal analysis

Thermal analysis in our study was accomplished by Differential Scanning Calorimetry (DSC). This technique was carried out to assess the thermal behavior of unprocessed Compound 30, PLGA, the physical binary mixture, and later the formed polymeric NPs. Samples (5 mg each) were weighed in aluminum pans using an empty open aluminum pan as a reference. The samples were placed in the DSC apparatus (Perkin-Elmer, model DSC-4, New York, NY) and heated in the range of 0–400 °C at a heating rate of 10 °C/min.

2.6. Preparation of drug-loaded NPs

PLGA-based NPs were prepared by nanoprecipitation method as reported by Katiyar et al. with some adjustments [22]. Briefly, PLGA was dissolved in acetone at two concentrations 1% and 0.6% (Table 1) and to this Compound 30 was added at a ratio of 1:10 of the dry polymer weight. Four milliliters of the obtained polymeric organic phase containing Compound 30 was added dropwise to 40 ml of aqueous phase having stabilizer (PVA or Tween 20) at a concentration of 2% w/v under magnetic stirring (Hot Plate and Magnetic stirrer, Misung Scientific Co., LTD, Korea). The flow rate of the organic phase was maintained at 0.6 ml/min using a 24-gauge needle attached to a syringe. By completing the addition of organic phase, the obtained mixture was placed in an ice bath and probe-sonicated using pulsed mode (on 2 s, off 1 s) for 5 min at 100% amplitude (Sonics Vibra cell, Sonic and Materials, Inc., USA). To enable the evaporation of acetone and leaving behind polymeric NPs dispersed in the aqueous phase, the obtained dispersion was stirred overnight. Before centrifugation, any agglomerates in the dispersion were removed by filtration through Whatman No. 1 filter paper, and the filtrate was separated at 11,000 rpm for 1 h (Benchtop Centrifuge, Sigma Laborzentrifugen, Germany). Then, NPs pellets were washed by DIW, collected, and stored at −20 °C. NPs were dried by lyophilization under reduced pressure and at −80 °C (Freeze dryer, SIM FD8-8T, SIM International, USA) and the resultant lyophilizates were stored at 4 °C for further valuation. Plain NPs (NP_P) were also prepared by the same steps mentioned above except for the Drug.

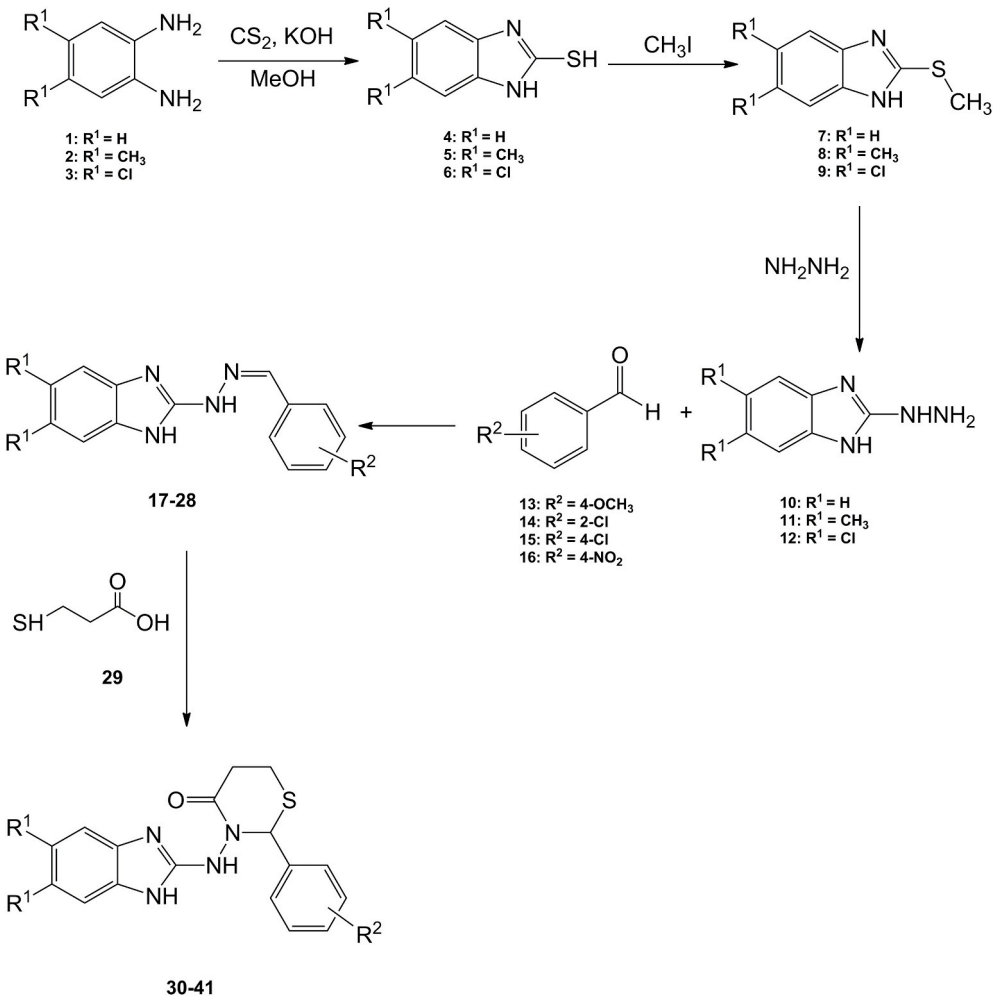

Scheme 1. Synthesis of the target compounds **30**–**41**.

2.7. Characterization of nanoparticles

2.7.1. Particle size, polydispersity index, and zeta potential

Average size (*Z-average*), polydispersity index (*PDI*), and zeta potential (ζ) of NPs were measured. The measurements were performed after appropriate dilution of aqueous dispersions of the prepared NPs with DIW at 25 °C (Zetasizer Nanoseries, Malvern Instruments Limited, UK). The measurements were repeated thrice, and the results were calculated as mean ± SD. Dynamic light scattering (DLS) and laser Doppler microelectrophoresis techniques were applied to *Z-average* and ζ measurements, respectively.

2.7.2. Morphology study

NPs shape and morphology were determined by transmission electron microscopy (TEM, JOEL 1010; JEOL Ltd, Tokyo, Japan). A ten-fold diluted drop of fresh NPs dispersion was positioned on a carbon-coated copper grid and left for 1 min to allow attachment of some NPs to the carbon substrate. Then, the extra dispersion was removed, and the grid was rinsed with DIW twice for a few seconds. After complete drying at room temperature, TEM photographs were captured directly without staining.

2.7.3. Encapsulation efficiency, loading efficiency, and percent yield

The percentage of Compound 30 encapsulation efficiency was estimated indirectly by determining the amount of free Compound 30 (non-encapsulated drug) in the supernatant of Drug-loaded NPs dispersion after centrifugation at 11,000 rpm for 1 h. Free Compound 30 was measured spectrophotometrically at 290 nm against the corresponding supernatant of NP_p as a blank. Plain supernatant was used to preclude any effect of the background. The encapsulation efficiency (*EE%*), the loading capacity (*LC%*), and percent yield (*Y%*) of the NPs were calculated [23].

2.7.4. In vitro release profiles and kinetic analysis

Release profiles of Compound 30 from Drug-loaded NPs (NP_3 and NP_4) and free Compound 30 were studied via vertical Franz diffusion cells with some modifications [24]. To serve as a release medium, 30 ml of $PB_{7.4}/MeOH_{20}$ were transferred to each receptor half-cell. Methanol was added to the release medium to maintain sink conditions [25]. Pre-equilibrated dialysis membrane (Spectra/Por® Dialysis Membrane, 12 KDa, Spectrum Laboratories, Inc., CA, USA) with area 3.8 cm^2 was used as a barrier to separate donor and receptor compartments. Then, NP_3, NP_4, and Free Compound 30 at amounts equivalent to 2 mg of Compound 30 were suspended in 2 ml of $PB_{7.4}$ and transferred to the donor compartments. To avoid evaporation of water, donor compartments were secured with wax foil (Parafilm® M, Bemis Company Inc., USA). In a shaking incubator at 37 °C ± 0.2 °C (GFL, Gesellschaft fur Labortechnik GmbH, Germany), triplicates of each diffusion cell were agitated at 100 rpm. Samples of receptor media were withdrawn at a prearranged schedule and replaced with an equivalent aliquot of fresh medium. The samples were passed through a 0.45 μm filter, appropriately diluted and their UV absorbances were measured at 290 nm. Concentrations of the Drug in the release media were determined at each time interval based on the standard curve that early constructed as

Table 2
Physicochemical characters of the synthesized compounds **30-41.**

Compound no.	R^1	R^2	T_M	Molecular Formula
30	H	4-OCH_3	245–6	$C_{18}H_{18}N_4O_2S$
31	H	2-Cl	169–71	$C_{17}H_{15}ClN_4OS$
32	H	4-Cl	142–6	$C_{17}H_{15}ClN_4OS$
33	H	4-NO_2	94–6	$C_{17}H_{15}N_5O_3S$
34	CH_3	4-OCH_3	146–50	$C_{20}H_{22}N_4O_2S$
35	CH_3	2-Cl	155–9	$C_{19}H_{19}ClN_4OS$
36	CH_3	4-Cl	166–9	$C_{19}H_{19}ClN_4OS$
37	CH_3	4-NO_2	123–7	$C_{19}H_{19}N_5O_3S$
38	Cl	4-OCH_3	181–6	$C_{18}H_{16}Cl_2N_4O_2S$
39	Cl	2-Cl	140–6	$C_{17}H_{13}Cl_3N_4OS$
40	Cl	4-Cl	169–73	$C_{17}H_{13}Cl_3N_4OS$
41	Cl	4-NO_2	102–8	$C_{17}H_{13}Cl_2N_5O_3S$

T_M; melting point in °C.

mentioned under the solubility section. The cumulative released concentration of the Drug at each time interval was calculated. Using the following mathematical models: zero-order; first-order, Higuchi equation [26], and Korsmeyer-Peppas equation [27], the acquired release data were kinetically analyzed. The principal model is the one with the maximum correlation coefficient (r^2) [28]. According to the acquired results, NP_4 was designated for the subsequent investigations.

2.8. Protein analysis of EZH2 and EpCAM in HEPG-2

HEPG-2 cells were cultured in a 6-well plate at a cell density of 10^5 cell/cm^2 using DMEM-high glucose with 10% FBS, 100 U/ml penicillin, and 100 μg/ml streptomycin at 37 °C in a 5% CO_2 incubator. When cells reached 90% confluency, FBS was decreased to 2% and cell treatment was conducted. The Drug was dissolved in DMSO and added to cells to reach a final concentration of 50 μM and 100 μM to represent Drug (50 μM) group and Drug (1000 μM) group, respectively with DMSO final concentration of 0.2% V/V in both groups. To serve as a control to Drug groups, additional cells were treated with DMSO only at the same concentration (DMSO group). On the other hand, NP_4 was dispersed in PBS, sonicated for 10 min, and then added to another cell lines with Drug equivalent concentration of 50 μM (NP_4 (50 μM) group) and 100 μM (NP_4 (100 μM) group). The polymer (PLGA) was used as a control by treating cells with amounts of polymer equivalent to those present in NP_4 (50 μM) group (Polymer (50 μM) group) and NP_4 (100 μM) group (Polymer (100 μM) group). Also, a control of untreated HEPG-2 cells was conducted (Control group).

After 72 h of incubation, representative phase-contrast images were taken. Cells in all groups were trypsinized, washed twice with PBS, then lysed using heat-freeze shock for EZH2 or specific kit extraction buffer for EpCAM measurements. Cell lysates were analyzed for EZH2 and EpCAM protein expression levels using ELISA Kits. Optical density was measured using a microplate reader (ROBONIK P2000-India). Experiments were done in triplicates and means were compared using one-way ANOVA with Tukey post-hock test. Statistical analysis was done using IBM SPSS Statistics for Windows, Version 25.0. Armonk, NY: IBM Corp.

3. Results and discussion

3.1. Chemistry results

The synthetic strategy for the synthesis of the target compounds is illustrated in Scheme 1. Starting with the preparation of 1*H*-benzo[*d*] imidazole-2-thiol derivatives **4-6** by the reaction of 1,2-diaminobenzen analogs **1-3** with carbon disulfide in presence of an alcoholic solution of potassium hydroxide. Compounds **4-6** were then S-alkylated with methyl iodide in acetone to produce compounds **7-9** that were treated with hydrazine hydrate to yield the 2-hydrazinyl-1*H*-benzo[*d*]imidazole derivatives **10-12**. Schiff's bases **17-28** were synthesized through the reaction of compounds **10-12** with a variety of substituted benzaldehyde

Table 3
Percent inhibition and IC_{50} (μM) of the synthesized compounds **30-41** against three human cancer cell lines.

Compound no.	% Inhibition*			IC_{50} (μM)		
	HEPG-2	MCF-7	PC-3	HEPG-2	MCF-7	PC-3
30	**64.0**	**50.8**	**36.7**	**8.95 ± 0.06**	**16.64 ± 0.4**	**27.04 ± 0.2**
31	**59.9**	**48.4**	**63.5**	**13.57 ± 1.4**	**20.32 ± 1.8**	**9.41 ± 0.8**
32	35.0	33.8	36.1	53.29 ± 2.3	74.32 ± 1.9	66.94 ± 1.1
33	21.8	24.9	18.6	55.81 ± 3.8	47.64 ± 3.5	64.57 ± 4.1
34	**42.6**	**41.7**	**40.3**	**68.27 ± 2.6**	**59.71 ± 3.8**	**66.29 ± 0.3**
35	36.5	37.0	35.2	79.27 ± 0.9	91.54 ± 1.1	72.68 ± 1.8
36	29.8	20.4	24.7	64.81 ± 3.9	82.47 ± 3.1	72.47 ± 2.2
37	**51.7**	**47.2**	**50.3**	**72.01 ± 2.9**	**93.48 ± 1.9**	**85.34 ± 3.3**
38	**48.6**	**47.3**	**48.2**	**68.65 ± 1.7**	**76.76 ± 3.3**	**71.75 ± 2.8**
39	33.6	31.5	34.2	55.39 ± 4.1	86.47 ± 3.0	63.38 ± 4.5
40	39.8	33.0	24.6	70.94 ± 2.7	84.36 ± 4.8	75.72 ± 3.8
41	**49.0**	**51.3**	**48.3**	**37.64 ± 2.2**	**42.84 ± 1.0**	**40.67 ± 5.1**
DOX	**72.7**	**74.1**	**62.1**	**4.50 ± 0.2**	**4.17 ± 0.2**	**8.87 ± 0.6**

HEPG-2, Human liver cancer cell line; **MCF-7**, Human prostate cancer cell line; **PC-3,** Breast cancer cell line; **DOX**, Doxorubicin, *The presented % inhibitions are at 12.5 μM.

13-16. The cyclization of Schiff bases was conducted through the reaction with thiopropionic acid **(29)** and yielded the tetrahydrothiazine derivatives **(30-41)**. All the newly synthesized compounds were subjected to structural elucidation by elemental analysis, NMR technique, and mass spectroscopy to confirm the structures of the synthesized compounds as shown in Table 2.

3.2. Screening of antitumor activity of the synthesized compounds

Table 3 documented the antitumor activity of the synthesized compounds expressed as IC_{50} and % inhibition at 12.5 μM. The synthesized compounds were subjected to screening against HEPG-2, MCF-7, and PC-3 to investigate their antitumor activity. By taking a closer look at the results obtained, it was revealed that the target derivatives **30-41** exerted promising activity against the selected cell lines. Among this series, compounds **30** and **31** are the most active derivatives with % inhibition values ranged from 36.7% to 64% and from 48.4% to 63.5%, respectively. At the same time, these two derivatives exerted the lowest IC_{50} values among all compounds with values in the range of 8.95–27.04 μM and 9.41–20.32 μM, respectively. Some of the compounds at the same series represent moderate % activity against the tested cell line such as compounds **34, 37, 38,** and **41** with values ranging 40.3%-51.7% and with IC_{50} values ranging from 37.64 to 93.48 μM. The rest of the compounds are considered inactive with low % inhibition value and high IC_{50} values. Hence, Compounds **30** and **31** were subjected to modeling.

3.3. Structure-activity relationship

It was found that the introduction of methoxy and chloro groups enhanced the antitumor activity giving the best results especially against HEPG-2 and MCF-7 cell lines with % Inhibition of 64%, 50.8% and 59.9%, 48.4% of compounds **30** and **31**, respectively (Tables 2 and 3).

Table 4
Best results of ligand docking with EZH2 subunit 3 as anti-tumor.

Reference drug	Compound 30	Compound 31
Tyr A661	Tyr A111	Tyr A661
Tyr A111	Tyr A661	Arg B236
Arg B236	Tyr A661	Asn A130
Leu A128	—	—

While it was noticed that the introduction of methyl group might result in moderate activities of some compounds such as **34, 38**, and **41** with % Inhibition ranging from 40.3% to 51.3%. The compounds having the lowest activity such as **36** and **40** were structurally similar in having either two chloro groups or one chloro group and one methyl group with % Inhibition ranging from 20.4% to 39.8%. It was also worth noting that the mono nitro derivative of the synthesized series **33** was showing weak antitumor activity with a % Inhibition of 21.8 against the HEPG-2 cell line. Upon the introduction of the methyl group along with the nitro group (compound **37**), the activity had shifted towards the direction of increasing the potency of the antitumor activity to % Inhibition of 51.7 against the same cell line (HEPG-2).

3.4. Molecular docking

Molecular docking permitted to determine the orientation of compounds and binding affinities at the active site of the PRC2. The protein-ligand complex was studied based on the X-ray crystal structure of PRC2. To investigate the possible binding mode of interactions, molecular docking was completed representing antitumor activity into subunit 3 of the PRC2 protein complex (EZH2). The recently solved X-ray crystal structure of the PDB ID: 5ls6 was used in our docking study.

Table 4 shows the binding of the reference drug and the selected compounds (**30** and **31**) with amino acids (similarities are underlined). 3D and 2D binding of Reference drug with pocket showed that Tyr A111 was a key amino acid (Fig. 1A and 1B). Compounds **30** and **31** were found to exhibit binding poses like those of the Reference drug occupying the binding cavity and, to varying extents. Compound **30** showed similarity in binding with Tyr A111 and Tyr A661 (2 bonds) which were all like the reference drug binding. Compound **31** showed similarity in binding with Tyr A661, Arg B236. Hence, docking results showed potential binding between Compound **30** and the key amino acid (Tyr A111). Reference drug and Compound **30** alignment is illustrated in Fig. 1C. Summing up all the above-mentioned findings, Compound **30** (Drug) was nominated as a promising EZH2 inhibitor to be loaded in PLGA-based NPs as drug delivery systems.

3.5. Preformulation study

3.5.1. T_M, solubility, and LogP of Compound 30

The determined value of T_M was found to be about 246 °C. Practically determined solubilities of Compound 30 were 1.02 ± 0.06 mg/ml (*Log*S = −2.54, 2.86 mM) and 1.86 ± 0.06 mg/ml (*Log*S = −2.28, 5.22 mM) in DIW and $PB_{7.4}/MeOH_{20}$, respectively. While the predicted aqueous solubility of Compound 30 was found to 0.165 mg/ml (*Log*S = −3.35, 0.463 mM). According to the USP solubility categorization, Compound 30 could be listed as slightly soluble (SS) (range of SS is from 1 to 10 mg/ml) [29]. If we rely upon the predicted aqueous solubility, Compound 30 can be shifted to the very slightly soluble (VSS) category (0.1–1 mg/ml).

For a molecule to dissolve in a solvent, it must be capable to dissociate from its solid crystal lattice by overcoming the intermolecular interactions with other neighboring molecules. Usually, T_M is used to determine whether compounds display solid-state-limited solubility or not [30]. Bergström and co-workers stated that compounds with T_M

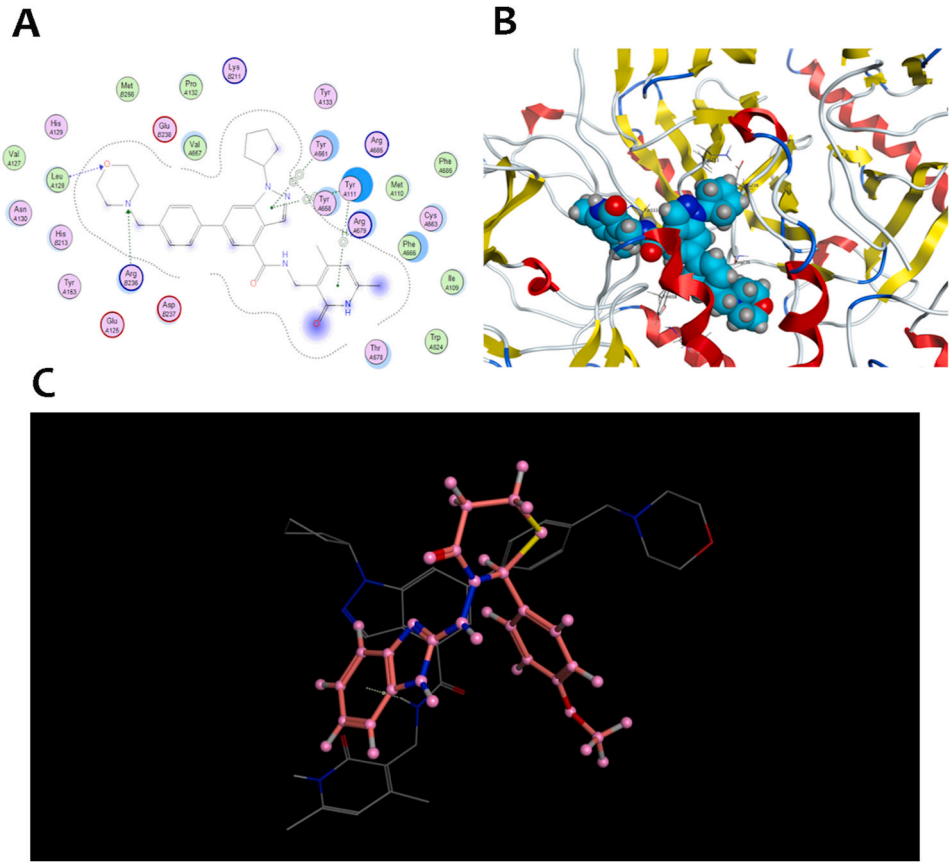

Fig. 1. Binding between reference drug and pocket 2D (A), 3D (B), reference drug, and Compound 30 alignment (C).

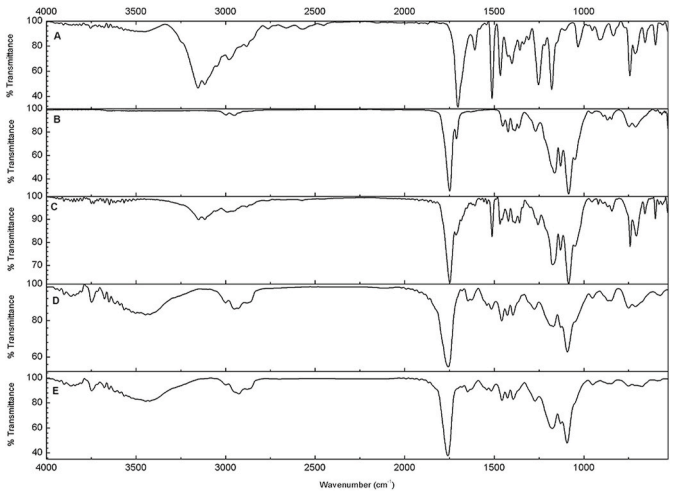

Fig. 2. FT-IR spectra of pure unprocessed Compound 30 (A), PLGA (B), the physical binary mixture (C), NP_3 (D), and NP_4 (E).

higher than 200 °C (T_M of Compound 30 = 246 °C) have strong crystal lattice that significantly influences their solubility [31]. Throughout the dissolution of a compound from its solid crystal lattice, the surrounding water molecules need to make a cavity for the incorporation of a new compound molecule within the aqueous environment. To decrease the energy accompanying cavity formation, some additives can be included in water to relax the tight junctions between its molecules with subsequent improvement of the solubility. Typically, such components are cosolvents (e.g., methanol). Such an explanation could be used to interpret the highly significant increase of solubility of Compound 30 in $PB_{7.4}/MeOH_{20}$ (*student t-test, P < 0.0001*). $PB_{7.4}/MeOH_{20}$ was used later as release media to impart sink condition. To sum up, Compound 30 can be considered as a poorly water-soluble compound.

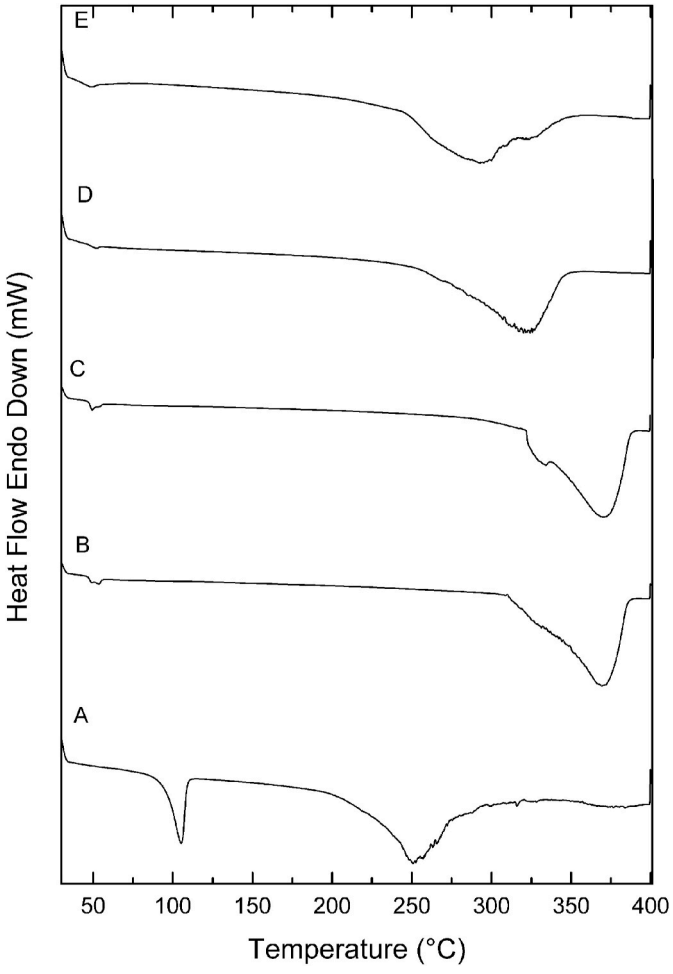

Fig. 3. Thermograms of pure unprocessed Compound 30 (A), PLGA (B), the physical binary mixture (C), NP_3 (D), and NP_4 (E).

Practically determined values of $K_{o/w}$ and *Log*P were 41.31 ± 3.1 and 1.62 ± 0.03, respectively. Comparable predicted values of $K_{o/w}$ and *Log*P were found values (50.12 and 1.7, respectively). Compounds could be classified according to their partition coefficients as the following; *Log*P < 1 (low lipophilicity), *Log*P in the range of 1–4 (intermediate lipophilicity) and *Log*P > 4 (high lipophilicity) [30]. Hence, Compound 30 could be considered as an intermediate lipophilic compound. In the background of pharmacokinetics, *Log*P can be valuable to predict the distribution profile of a drug *in vivo* which in turn has a great impact on its absorption, distribution, metabolism, and elimination (ADME). *Log*P as well helps to decide the most possible route of administration. For orally absorbed drugs, they must pass first across lipid bilayers of the intestinal epithelium. Consequently, a certain level of lipophilicity is essential to allow partitioning of the drug to the bilayer. At the same time, the drug requires some hydrophilicity so that it will partition out again to the aqueous environment of systemic circulation [32].

The modified general solubility equation (GSE) also displayed the effect of *Log*P and T_M on the solubility of a compound [33].

$$LogS = 0.5 - 0.01(T_M - 25) - LogP$$

Where *Log*S is the solubility, T_M is the melting point and *Log*P is the partition coefficient. In that way, it was proven that there is a direct relationship between the partition coefficient of a compound and its solubility. The solubility of compounds with *Log*P < 2 (*Log*P of Compound 30 = 1.62) is principally dependent on their solid state. It is believed that the drug development process of such compounds, which are especially solubility-limited due to their solid states, is going smoothly and terminated relatively early. Such findings had encouraged us to go forward in our drug development steps of Compound 30. Any strategy that can change the solid crystal form could be beneficial for increasing the rate of dissolution and attaining enhanced apparent solubility [34]. As a rule, amorphous solid dispersions can offer high bioavailability for drugs suffering from low solubility. Very high surface area dispersions, such as Drug-loaded NPs, are principally well appropriate to rapid-onset applications owing to their initial fast release rate [35]. Furthermore, the observed amorphous nature of NPs could impart higher concentrations of the dissolved drug than crystalline solubility. Such a feature might contribute to faster and higher absorption rates [36].

3.5.2. FT-IR

FT-IR is mainly used to measure the selective absorption of light by the vibration pattern of specific chemical bonds. Such observation could permit assessing any kind of interaction that might occur between drug and polymer. In the case of interaction, the vibrations of the atoms involved in this interaction can suffer modifications in frequency and intensity [37]. Fig. 2 shows the FT-IR spectra of pure unprocessed Compound 30 (A), PLGA (B), the physical binary mixture (C), NP_3 (D), and NP_4 (E) that were studied to assess the interaction between the Compound 30 and the PLGA [18].

For the spectrum of Compound 30 (Fig. 2A), stretching of N–H and aromatic C–H exhibited at 3450 cm^{-1} and 3116 cm^{-1}, respectively. Small peaks at 2571 cm^{-1} and 2660 cm^{-1} represented S–H vibration. While sharp peaks at 1402 cm^{-1} and 1254 cm^{-1} displayed C–N stretching. Stretching of C═N in the imidazole ring and amide C═O in the thiazinanone ring appeared at 1466 cm^{-1} and 1703 cm^{-1}, respectively. The vibrational peak at 1179 cm^{-1} could be assigned to the methoxy C–O bond. Stretching of C═C appeared at 1609 cm^{-1} and C–C

appeared at 1308 cm^{-1} and 1357 cm^{-1}. Methyl group vibration exhibited at 2882 cm^{-1} and 2981 cm^{-1}. Fig. 2B displays several major peaks in the FT-IR spectrum of PLGA. The carbonyl (C═O) group of the PLGA appears at 1749 cm^{-1}. Also, bending vibration of the aliphatic $–CH_3$ and $–CH_2$ groups appear at 1453 cm^{-1}, 1384 $cm^{-1,}$ and 1270 cm^{-1}, whereas the bands at 1180 cm^{-1} and 1085 cm^{-1} could be related to the stretching of the ester C–O–C. Absorption peaks between 2850 cm^{-1} and 3000 cm^{-1} were assigned to stretching vibrations of aliphatic C–H. The spectrum of Compound 30 and PLGA physical mixture (Fig. 2C) shows both the characteristic peaks of Compound 30 and PLGA that presented above in their spectra without major shifts. The only decrease in the intensity of the peaks could be observed in the spectrum of the physical mixture. This indicated that there was no interaction between Compound 30 and PLGA. Fig. 2D and E shows the FT-IR spectra of NP_3 and NP_4, respectively. The characteristic peaks of Compound 30 at lower intensity could be observed due to its proportion in the formulation. The above-mentioned results revealed computability between Compound 30 and PLGA and at the same time indicated the ability to incorporate Compound 30 in the PLGA polymeric matrix of NPs.

3.5.3. DSC

Thermal analysis via DSC was accomplished to define any possible alteration in the physical features of the components individually and to evaluate crystalline or amorphous behavior of Drug-loaded NPs [38]. Such study of phase transition could specify the potential changes in the crystallinity of Compound 30 that might affect both *in vitro* release and *in vivo* cellular uptake [39]. As the crystalline form needs more energy to separate into the well-organized molecules, low aqueous solubility and consequently low physiological bioavailability might have arisen. However, randomly arranged molecules of the amorphous state need low energy to separate and this situation might be followed by superior bioavailability [15].

Fig. 3 shows the thermograms of pure unprocessed Compound 30 (A), PLGA (B), the physical binary mixture (C), NP_3 (D), and NP_4 (E). A DSC thermogram of Compound 30 presents two endothermic peaks at 105.34 °C and 250.72 °C that could be related to the liberation of physically-bound water (evaporation of moisture content) and the melting point of Compound 30, respectively (Fig. 3A). The previously determined T_M was found to be much closer to that exhibited by thermal analysis of Compound 30. Such a finding demonstrated the crystallinity of Compound 30 in its molecular structure. Another small endothermic peak appeared at 316 °C that could be correlated to the decomposition of Compound 30. Fig. 3B shows the thermogram of PLGA with two endothermic peaks at 53.33 °C and 369.47 °C representing polymer its glass transition and its thermal decomposition, respectively. It was reported that the glass transition of PLGA happened at the 48–55 °C range, with a midpoint value at 52 °C. No melting point was detected, due to the amorphous nature of PLGA [37]. For the binary mixture of Compound 30 and PLGA, it could be observed that the characteristic peaks of PLGA and decomposition peak of Compound 30 were not affected by their physical blending (Fig. 3C). In the Drug-loaded NPs thermograms, PLGA peaks were identified while endothermic peaks of Compound 30 were completely disappeared (Fig. 3D and E). This indicated that the incorporation of Compound 30 in NPs transformed its physical state from crystalline to amorphous one. Therefore, it could be proven that Compound 30 was completely loaded in an amorphous state because of the complete dissolution of its crystals in the PLGA-based polymeric matrix. Hence, Compound 30 remained dispersed at the molecular level in the solid dispersion after the formation of NPs [39].

3.6. Characterization of nanoparticles

3.6.1. Preparation of drug-loaded polymeric nanoparticles

Among the numerous approaches used in the preparation of NPs, the nanoprecipitation technique was selected. In this technique, polymer (PLGA) and Compound 30 (Drug) are dissolved in an organic phase, which is further added to an aqueous phase containing a stabilizer. Physical coating of polymer surface by the stabilizer imparts a hydrophilic stealth character to stabilize polymeric NPs [40]. Although chlorinated solvents such as methylene chloride and chloroform have been comprehensively used to dissolve the PLGA, acetone was used. Acetone has a low boiling point (56 °C) with relatively low toxicity and it is completely miscible with water [41]. Upon the organic phase-dropping, droplets are promptly stabilized and then acetone started to diffuse out of the organic droplets to the surrounding aqueous medium due to their mutual miscibility. Such a condition creates interfacial turbulence followed by precipitation of PLGA that finally resulted in the formation of NPs [42].

For the Drug-loaded NPs, Compound 30 was incorporated at a ratio of 1:10 of the dry polymer weight. Using a similar ratio of 1–10, the organic phase was dropped into the aqueous phase containing the stabilizer (2% w/v). During the preparation of the Drug-loaded NPs, it was observed that PLGA of NP_1 and NP_2 almost had separated from the preparation medium as coarse agglomerates without the formation of NPs. Hence, Tween 20 was more efficient than PVA as a stabilizer and it greatly enhanced the formation of NPs (NP_3 and NP_4). Due to its high hydrophilic-lipophilic balance (HLB) value of 16.7, Tween 20 has adsorbed on the interface to contribute to further reduction of surface tension and facilitate dispersion of organic phase in aqueous one [43]. Therefore, Tween 20 could participate in the coverage and cause stabilization of newly formed NPs [44]. As a result, our effort was directed for further preparation and characterization of Tween 20-stabilized NPs (NP_3 and NP_4).

3.6.2. Z-average, PDI, and ζ potential

Z-average of NP_3 and NP_4 were determined using the DLS technique and were found to be 252.2 nm and 256.2 nm, respectively (Table 1). The determined *Z-average* was found to be within the nano-range of <1,000 nm. Moreover, it could be observed that increasing polymer concentration by about 40% (NP_3) had not significantly affected the *Z-average*. Mainly, particle size significantly participates in determining the biofate of NPs *in vivo*. Very small NPs (<10 nm) can be quickly cleared from the general circulation by renal filtration. While NPs with a diameter higher than 200 nm have the potential to be entrapped in the reticuloendothelial system (RES)-rich organs such as the liver [45]. NPs with reduced mean particle size (<300 nm) are more appropriate for drug release and transport in the bloodstream, extravasation, and accumulation in the interstitial space of the tumor cell (EPR effect) with passive targeting [46]. Nevertheless, the transport mechanism of NPs, the pore cutoff size of numerous tumors has been described to range between 380 and 780 nm [47]. Among different sized nanocarriers, a maximum particle size of 400 nm was suggested to be suitable for extravasation into tumors [48]. Some studies have revealed that NPs with particle sizes lower than 200 nm are more effective for tumor extravasation [49].

The measured values of *PDI* were less than 0.2. Where 1 is the maximum value and 0 is the lowest of PDI; the higher the PDI value designates NPs to have a variable size range with poor homogeneity and low stability. Small PDI (<0.4) is appropriate because such a value suggests narrow size distribution. Henceforth, the obtained PDI values of prepared Drug-loaded NPs indicated a narrow distribution profile that could realize the EPR effect, and play an imperative role in tissue accumulation and renal clearance [18]. To sum up, the obtained values of *Z-average* and PDI were in the acceptable range and further evaluation could be conducted.

An additional factor that plays a vital role in biodistribution and uptake is the surface charge of the NPs which is usually measured in the form of zeta potential (ζ potential). Table 1 documented that NPs had negative ζ potential (−10.04 mV and −16.58 mV). The negative ζ values could be attributed to the terminal carboxyl groups of PLGA that lead to negatively charged particle surfaces [50]. The surface charge shows a

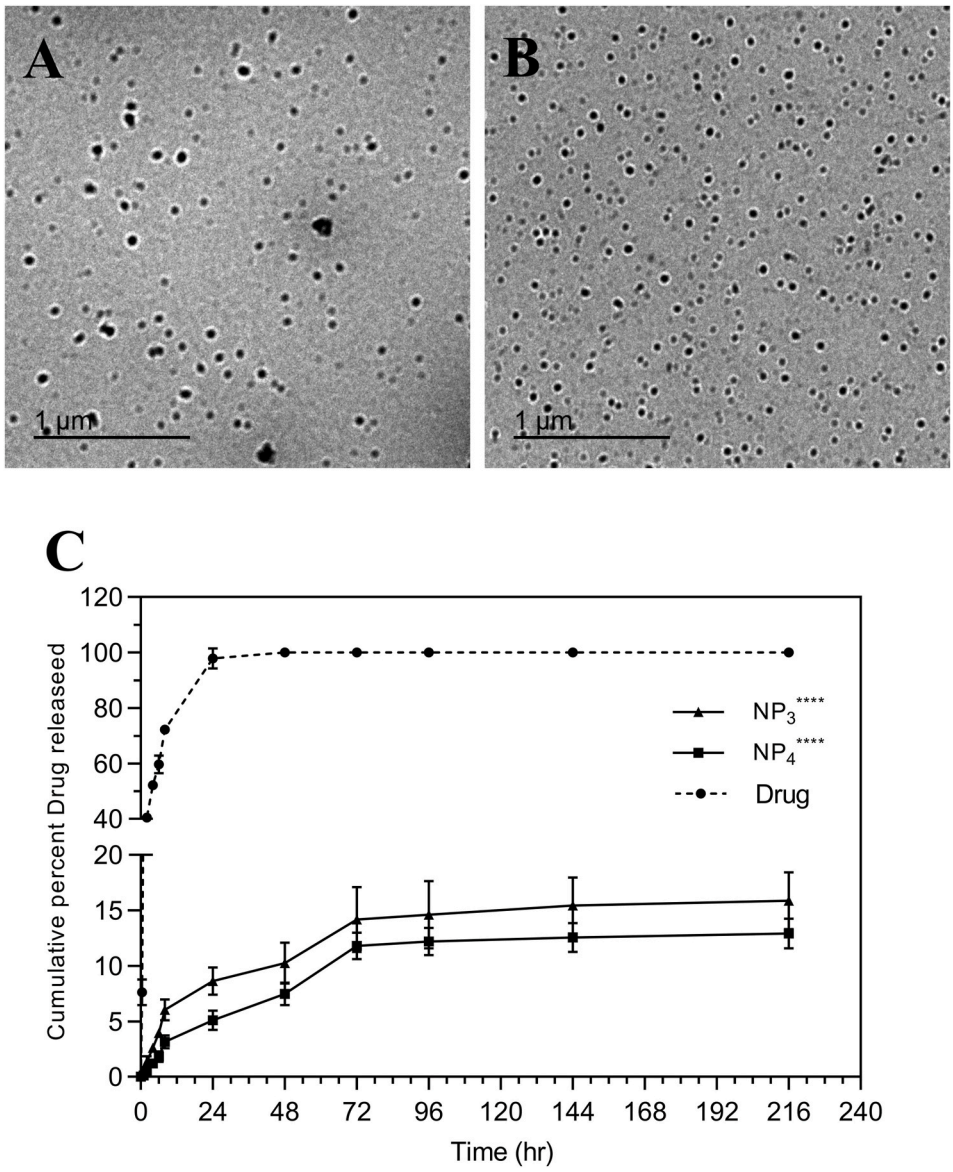

Fig. 4. TEM images of NP_3 (A), NP_4 (B), and *in vitro* release profiles (C). Release data displayed as mean ± SD; n = 3, ***$P < 0.001$.

critical role in cellular uptake through a two-step process, binding of NPs with cell membrane and internalization inside cells. Also, The ζ potential is a sign of the colloidal suspension stability [51]. The negative ζ potential of NPs could cause repulsion among them which in turn might result in precluding their aggregation [52]. Even though positively charged NPs have displayed superior internalization *in vitro*, they can easily bind other healthy cells such as endothelial cells, before reaching the target tumor cells. Thus, it is empirical to keep the NPs as neutral or negatively charged as possible [53]. Besides, positively charged NPs have presented a dose-dependent hemolytic activity while negatively charged ones did not [17]. Surface characteristics also affect the biofate of NPs in the systemic circulation [54]. Longer circulation half-life and less clearance were exhibited by neutral and negatively charged NPs [55].

3.6.3. Morphology study

The morphology and the structure of NP_3 and NP_4 had been investigated by TEM images as shown in Fig. 4A and 4B, respectively. Both formulations showed spherical and uniform structure nanosized particles with a smooth surface. Zhang and co-workers reported that spherical-shaped NPs are more readily to be engulfed by cells than other shapes [56]. The TEM image also verified that NPs did not exhibit aggregation and at the same time had a narrow particle distribution. By matching DLS-measured *Z-average* with a particle size that was observed by TEM, a higher value was exhibited by the DLS technique. The analogous finding was documented in several studies. Such a situation could be attributed to the hydrodynamic *Z-average* of NPs rather than the true physical size of individual particles was determined by the DLS technique [57]. Hence, we thought that the actual particle size of the prepared NPs might be smaller than 250 nm (*Z-average*).

3.6.4. Encapsulation efficiency, loading efficiency, and percent yield

EE%, *LC%,* and *Y%* of NP_3 and NP_4 are listed in Table 1. It could be noted that loading of Compound 30 in NP_4 (35.41%) significantly enhanced its *EE%* to more than two folds that of NP_3 (14.9%). In the same manner, NP_4 exhibited better values of *LC%* and *Y% (*4.15% and 46.19%, respectively) than corresponding ones of NP_3 (1.56% and 18.14%, respectively). From our findings, it was evident that increase PLGA concentration was associated with a reduction of *EE%, LC%,* and *Y %* of Compound 30. Tween 20 is a smaller surfactant molecule, which effectively stabilizes NPs by the formation of a thin protective outer layer followed by a decrease of interfacial tension. For NP_3, the thin

Table 5
Kinetic analysis of Drug released from its suspension, NP_3 and NP_4.

Correlation coefficient (r^2)	Formulation Code		
	Drug	NP_3	NP_4
Zero	0.7455	0.8081	0.9265
First	0.9856	0.8185	0.9318
Higuchi	0.9455	0.9443	0.9746
Release order	First	Higuchi	Higuchi
K–P r^2	0.8534	0.8776	0.9557
n	0.59	0.84	0.85
Main mechanism		Non-Fickian diffusion	

layer might be insufficient to wet the excessive amount of Compound 30 (40% higher than NP_4) which probably led to a decrease encapsulation capability of Tween 20 [58].

3.6.5. *In vitro* release profiles and kinetics

The *in vitro* release studies were performed using a dialysis membrane that simulates the ultimate performance in the biological fluids. Phosphate buffer containing 20% (V/V) methanol ($PB_{7.4}$/$MeOH_{20}$) was used as a release medium to provide sink conditions as well as bypassing the interfering effect of Compound 30 low solubility [59]. In the sink phase, a drug concentration has to be kept at less than 10% of its saturation solubility [60]. The effectiveness of the release study design could be ensured by checking the release of the Drug from its unprocessed naked form. The release pattern of the Drug from its suspension, NP_3, and NP_4 are shown in Fig. 4C. The free Drug was almost released within 24 h. This could certify that the dialysis membrane could allow passage of Compound 30 molecules through its pores. As exhibited, both NPs formulations demonstrate an initial burst release during the first 72 h of incubation (Fig. 4C). This initial burst release observed in our study has been commonly perceived in many studies of the polymeric NPs [11]. This initial burst could be related to Compound 30 molecules embedded at the outermost layers of the polymeric matrix and those adsorbed on the surface of NPs. The initial burst was followed by a sustained-release pattern for both types of NPs. The sustained release could be attributed to the fraction of Compound 30 that entrapped within the core of NPs. Furthermore, slow degradation of PLGA principally causes further sustained release of the Drug. Hence, the obtained release behavior is likely to be a biphasic release. The *in vitro* release after 216 h had resulted in overall 16% and 13% Drug depletion from NP_3 and NP_4, respectively. However, the burst effect is advantageous to get a rapid onset of a drug at the action site, as well as the prolonged release is essential to uphold the drug effects [15]. It could be observed that the percent released of the Drug from NP_3 and NP_4 was significantly lower than the corresponding value of the Drug alone (Drug suspension) along the release time ($P < 0.001$). The PLGA-based polymeric matrix of NPs was thought to be responsible for the observed rate-controlling manners of NP_3 and NP_4. In tumor therapy, attaining sustained drug release played an extra important role in improving the curative effect, preventing tumor cells to be subjected to a massive concentration of a drug and hence precluding the development of therapy resistance [61]. For further interpretation of our results, *in vitro* release data were fitted to different mathematical models to be kinetically analyzed.

Studying kinetics of drug release is essential as it has correlated the *in vitro* and *in vivo* drug responses by relating outcomes of pharmacokinetics and release patterns. Different models could be applied, the most well-matched being the one that best fits the release data. Table 5 shows correlation coefficients (r^2) that are used to define the best fitting model. It was found that the release of the Drug from NP_3 and NP_4 was best fitted for the Higuchi model with r^2 values of 0.9443 and 0.9746, respectively. Such a finding suggested a diffusion-driven release mechanism of the Drug from the prepared NPs. To understand the release mechanism in-depth, release data were fitted to the Korsmeyer-Peppas exponential model. The diffusional release exponent (n) of NP_3 and NP_4 were 0.836 and 0.85, respectively which designated that they exhibited a non-Fickian or anomalous diffusion ($0.5 < n < 1$). This means that Drug release from the prepared NPs was not governed by pure diffusion mechanism but is rather a combination of Drug diffusion through NPs and erosion of the polymeric matrix. On the other hand, it was found that the release of the Drug from its suspension followed first-order kinetics which means that the release of pure Compound 30 was dependent on its concentration in the donor compartment. Based on the above-mentioned characterization, NP_4 was selected to be subjected to further evaluation and development.

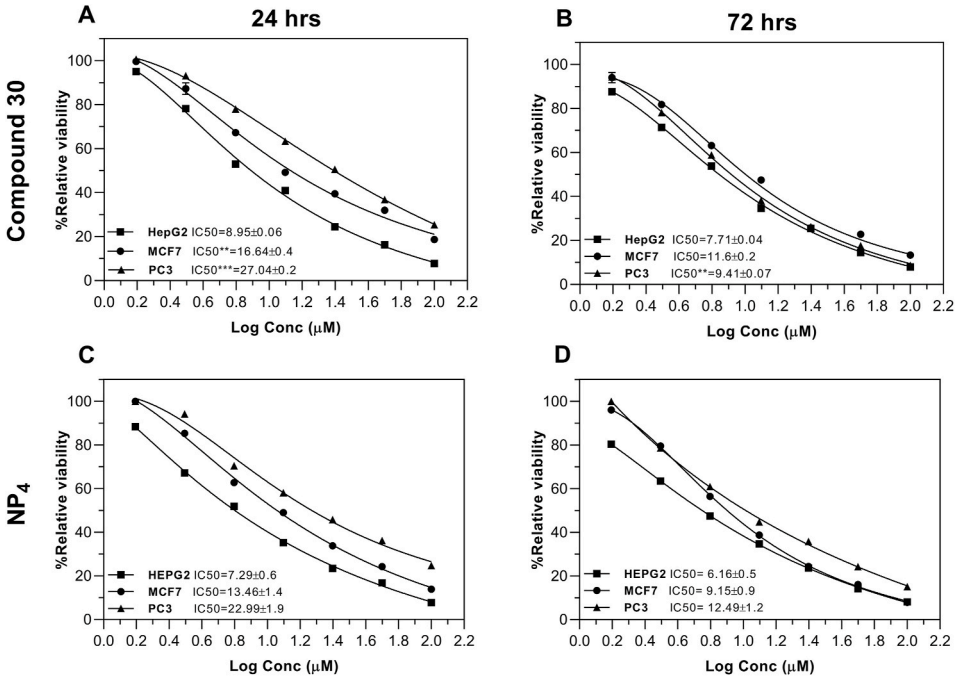

Fig. 5. Relative viability of HEPG-2, MCF-7, and PC-3 cell lines after incubation with serial concentrations of Compound **30** and NP_4 for 24 h and 72 h. Data displayed as mean ± SD; n = 3, *$P < 0.05$, * *$P < 0.01$, and ***$P < 0.001$.

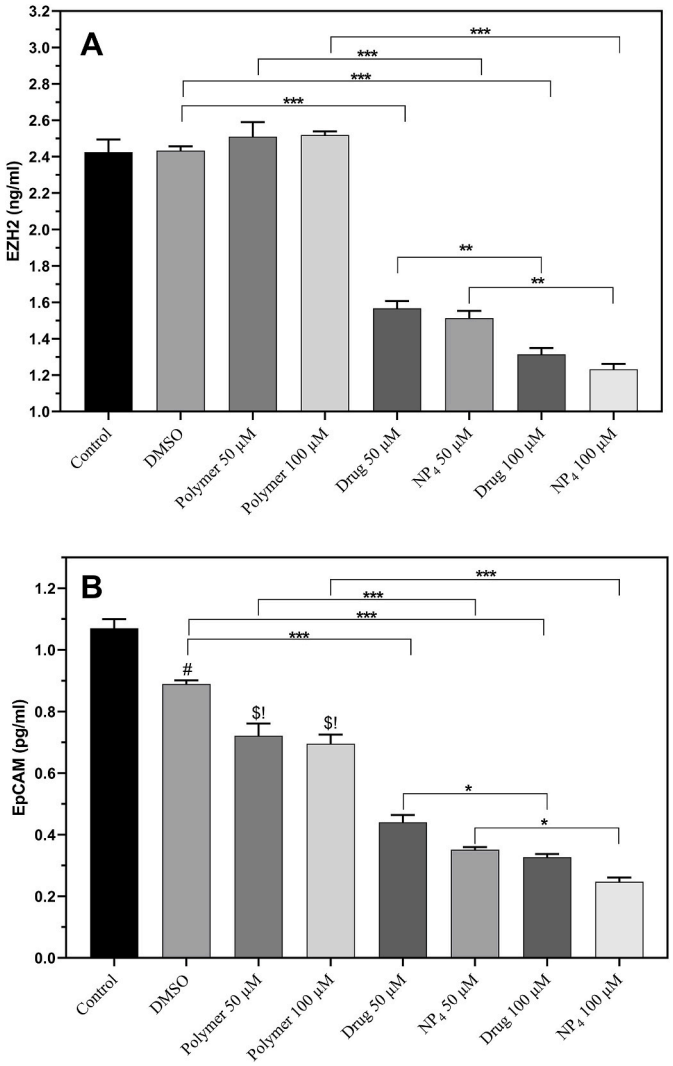

Fig. 6. Protein expression level of EZH2 (ng/ml) and EpCAM (pg/ml) in cell lysates of different groups. Data displayed as mean ± SD; n = 3, $^{*}P < 0.05$, $^{**}P < 0.01$, $^{***}P < 0.001$, $^{\#}P < 0.05$ Vs the control group, $^{\$}P < 0.001$ Vs the control group, $^{!}P < 0.01$ Vs the DMSO group.

3.7. In vitro antitumor activity of Compound 30 and NP_4

Fig. 5 shows the *in vitro* antitumor activity of Compound 30 and NP_4, respectively expressed as means relative viability of HEPG-2, MCF-7, and PC-3 cell lines after incubation with different concentrations for 24 h (right panel) and 72 h (left panel). It was found that Compound **30** reduced the cell viability of all tested cell lines. It could be observed that the most sensitive cell line was HEPG-2 with IC_{50} values of 8.95 μM and 7.71 μM after 24 and 72 h of incubation, respectively (Fig. 5A and B). The least sensitive cell line after 24 h was PC-3 with $IC_{50} = 27.03$ μM. However, MCF-7 was the least sensitive one with $IC_{50} = 11.6$ μM after 72 h of incubation (Fig. 5B). It was found that Drug-loaded NPs (NP_4) also diminished cell viability of the tested cancer cell lines as shown in Fig. 5. Similarly, HEPG-2 was the most sensitive cell line with IC_{50} values 7.29 μM and 6.16 μM after 24 and 72 h of incubation, respectively. On the other hand, the PC-3 cell line exhibited the highest resistance with IC_{50} values of 22.99 μM and 12.49 μM after 24 and 72 h, respectively (Fig. 5C and D). Compound **30** showed much higher IC_{50} values (81.01 ± 12.93 and 62.63 ± 4.52 μM after 24 h and 72 h; respectively) against THLE-2 cells compared to HEPG-2 (Fig. SI-1). These data suggest that Compound **30** might have a selective enhanced cytotoxic effect against the tumor cells. A safe concentration range for future *in vivo* studies should be determined before commencing studies. To sum up, the results indicated that Compound 30 decreased the viability of the tested cancer cell lines with reasonable IC_{50} values. Furthermore, Compound **30** showed promising antitumor activity versus HEPG-2. At the same time, the incorporation of Compound **30** in polymeric PLGA-based NPs (NP_4) had not retarded its antitumor activity. HEPG-2 was the most sensitive for either Compound **30** or NP_4. Hence, further evaluation was directed towards focusing on protein expression levels of HEPG-2 (HCC).

3.8. EZH2 and EpCAM protein expression

Fig. 6A and B shows the protein expression levels of EZH2 and EpCAM, respectively. The Drug displayed a potent inhibitory effect on the EZH2 protein expression and reduced its level by ≈ 1.5 fold at 50 μM and ≈1.8 fold at 100 μM concentration compared to the DMSO group. Also, NP_4 decreased the EZH2 expression by ≈ 1.6 fold at 50 μM and ≈2 fold at 100 μM concentration compared to the respective polymer controls. The EpCAM protein expression in cell lysate decreased by ≈ 2 fold in Drug (50 μM), ≈2.7 fold in Drug (100 μM), ≈2 fold in NP_4 (50 μM), and ≈2.8 fold in NP_4 (100 μM) groups. Consistently, statistical analysis revealed that the Drug at 50 μM and 100 μM significantly reduced protein expression levels of EZH2 and EpCAM in comparison to the DMSO group ($P < 0.001$) and Control group ($P < 0.001$). Similarly, NP_4 at both concentrations showed a significant decrease in EZH2 and EpCAM levels compared to the corresponding ones of polymer groups ($P < 0.001$), respectively.

It was observed that the decrease in EZH2 protein expression had occurred in a dose-dependent manner (Fig. 6A). This finding was verified by the noticeable significant differences between EZH2 expression levels of Drug and NP_4 groups at 100 μM and the corresponding ones at 50 μM ($P < 0.01$). Moreover, EpCAM protein expression levels showed a similar dose-dependent pattern (Fig. 6B). Drug and NP_4 groups at 50 μM demonstrated significantly higher EpCAM levels than the corresponding groups at 100 μM ($P < 0.05$). On the other hand, it was found that treating the cells with 50 μM or 100 μM of NP_4 decreased the protein expression levels insignificantly when compared to the corresponding Drug groups, ($P > 0.05$). There was no significant change between the EZH2 expression levels in the Control group compared to either DMSO, Polymer (50 μM), or Polymer (100 μM) groups. Interestingly, DMSO significantly decreased EpCAM levels compared to the Control group ($P < 0.05$). Besides, both Polymer groups showed a significant decrease in EpCAM levels compared to either the Control group ($P < 0.001$) or the DMSO group ($P < 0.01$). The ability of DMSO to lessen EpCAM expression in HEPG-2 could be attributed to its reported epigenetic and *in vitro* catalytic activities on DNA methyltransferase 3a [62].

Fig. 7 illustrates phase-contrast images of HEPG-2 cell line of different groups after 72 h. The control group (Fig. 7A) exhibited normal cell morphology with typical viability. The Drug (50 μM) group showed senescent and dead cells while most HEPG-2 cells treated with 100 μM Drug were dead with a marked decrease of cell number (Fig. 7C and D, respectively). Cells of both Polymer groups at 50 μM and 100 μM, which were shown in Fig. 7E and F, respectively demonstrated some dead cells. Treatment of HEPG-2 with NP_4 at a concentration of 50 μM caused an obvious decrease in cell viability (Fig. 7G). NP_4 (100 μM) group incorporating a higher concentration of the Drug offered nearly complete cell death (Fig. 7H).

Our results could be interpreted considering the below-mentioned details. Embryonic-stage active genes are known to be silenced in adulthood by several mechanisms with the chromatin-modifying PRC2 being at the core of the silencing mechanism. Dysfunction of PRC2 leads to reactivation of developmentally regulated genes and has been associated with several types of tumors. EZH2 or enhancer of zeste 2 is a catalytic subunit of PRC2. EZH2 and its associated PRC2 complex are the most significantly deregulated epigenetic regulators in primary HCC [63]. The overexpression of EZH2 in cancer cells leads to independent

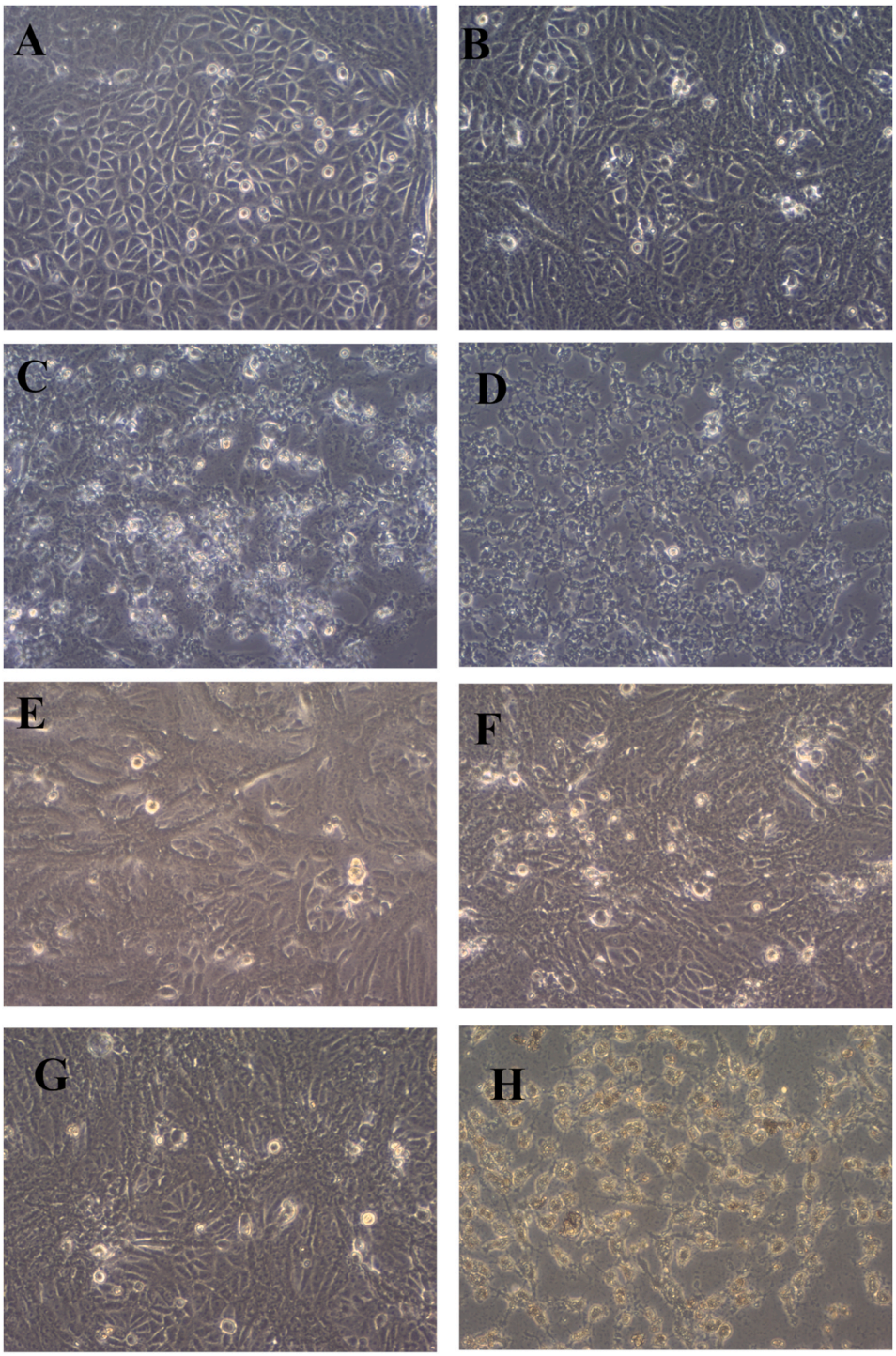

Fig. 7. Phase contrast images of HEPG-2 cell line after 72 h of incubation of Control (A), DMSO (B), Drug 50 μM (C), Drug 100 μM (D), Polymer 50 μM (E), Polymer 100 μM (F), NP_4 50 μM (G) and NP_4 100 μM (H) groups. Scale Bar: 100 μm.

methylation and Wnt/β-catenin signaling activation and finally increased EpCAM expression [64]. Depletion of β-catenin from mature hepatocytes initiated active proliferation to replace hepatocytes with new ones expressing β-catenin and EpCAM leading to an expansion of hepatic progenitor cells and tumor development [65].

EpCAM expression in HCC is believed to mark cancer cells with epithelial-mesenchymal transition capability; i.e; cancer stem cells. Eventually, this leads to increased tumor malignancy and worsens the prognosis [66]. Based on their EZH2 inhibitory effect, both Drug and NP_4 decreased EpCAM expression in HEPG-2. Additionally, Drug and NP_4 might decrease the possibility of metastasis or tumor relapse after chemo/radiotherapy due to their ability to eradicate $EpCAM^+$ cancer stem cells. Such findings indicated that Drug and NP_4 had targeted EZH2 and the downstream signaling pathway that leads to a decline of EpCAM expression as well as HEPG-2 cell viability.

In the literature, the scholars had focused on the synthesis of different EZH2 inhibitors without further processing towards further pharmaceutical and biological applications [15–18]. Hence, the practicability, applicability, and sustainability of the developed compounds are thought to be impaired in the field of pharmacy. In our study, EZH2

inhibitors had been designed, synthesized, and screened for their antitumor activity. Then, our work was extended to energize the docking study for investigating the potential mechanisms of action and select the most appropriate compound (Compound **30**). The physicochemical properties of Compound **30** were studied before incorporation into the polymeric nanoparticles. Full characterization of Compound **30** in its pure and nano-form was conducted including *in vitro* release, antitumor activity, and protein expression levels of EZH2 and EpCAM. Instead of just creating the compounds followed by their initial evaluation, the presented study sections had been organized to allow the smooth flowing of the results from a specific working area to be functionalized in another one.

Up to our knowledge, this study is one of the few studies that dealt harmonically with the application of all these areas in the pharmaceutical field. The obtained outcomes indicated that the newly synthesized EZH2 inhibitor can be considered a promising antitumor drug. Moreover, our results also offered us another evidence in favor of the use of polymeric PLGA-based NPs as a delivery system of Compound 30. Moreover, a plan of a future study has been designed to include further work regarding *in vitro* targeting of EZH2, *in vivo* evaluation, and screening of various possible pathways of Compound 30 and NP_4 that can be disrupted in malignancy.

4. Conclusion

EZH2 is a histone-lysine N-methyl transferase enzyme that its upregulation is linked to the overexpression of EpCAM. In our study, a new series of benzimidazole derivatives were synthesized, characterized, and screened for their antitumor activity. Also, modeling studies were performed to investigate their ability to target EZH2. Among synthesized derivatives, Compound 30 was incorporated into a novel drug delivery system (NP_4). Results of *in vitro* antitumor activity revealed that HEPG-2 was the most sensitive for Compound 30 or NP_4. Protein analysis indicated that Compound 30 and NP_4 had targeted EZH2 and its downstream signaling pathway. In the future, *in vivo* antitumor studies can be conducted to extensively recognize the biofates of Compound 30 and NP_4 in the treatment of HCC.

Author contribution

Ghada S. Hassan, Sara T. Al-Rashood and Dr. Noha M. Saleh designed research; Hoda A. Elkot, Ibrahim Ragab, Noha M. Saleh, Mohamed N. Amin achieved research practical work; Shahenda M. El-Messery performed molecular modeling; Ghada S. Hassan, Shahenda M. El-Messery, Noha M. Saleh, Mohamed N. Amin analyzed data and wrote the paper.

Declaration of competing interest

The authors declare that they have no known competing financial interests or personal relationships that could have appeared to influence the work reported in this paper.

Appendix A. Supplementary data

Supplementary data to this article can be found online at https://doi.org/10.1016/j.cbi.2021.109530.

References

[1] S. Sharma, T.K. Kelly, P.A. Jones, Epigenetics in cancer, Carcinogenesis 31 (2010) 27–36, https://doi.org/10.1093/carcin/bgp220.

[2] Y.G. Zheng, J. Wu, Z. Chen, M. Goodman, Chemical regulation of epigenetic modifications: opportunities for new cancer therapy, Med. Res. Rev. 28 (2008) 645–687, https://doi.org/10.1002/med.20120.

[3] S.R. Thornton, V.L. Butty, S.S. Levine, L.A. Boyer, Polycomb repressive complex 2 regulates lineage fidelity during embryonic stem cell differentiation, PloS One 9 (2014), e110498, https://doi.org/10.1371/journal.pone.0110498.

[4] K. Xu, Z.J. Wu, A.C. Groner, H.H. He, C. Cai, R.T. Lis, X. Wu, E.C. Stack, M. Loda, T. Liu, H. Xu, L. Cato, J.E. Thornton, R.I. Gregory, C. Morrissey, R.L. Vessella, R. Montironi, C. Magi-Galluzzi, P.W. Kantoff, S.P. Balk, X.S. Liu, M. Brown, EZH2 oncogenic activity in castration resistant prostate cancer cells is polycomb-independent, Science (New York, N.Y.). 338 (2012) 1465, https://doi.org/10.1126/science.1227604.

[5] S.K.K. Mani, H. Zhang, A. Diab, P.E. Pascuzzi, L. Lefrançois, N. Fares, B. Bancel, P. Merle, O. Andrisani, EpCAM-regulated intramembrane proteolysis induces a cancer stem cell-like gene signature in hepatitis B virus-infected hepatocytes, J. Hepatol. 65 (2016) 888–898, https://doi.org/10.1016/j.jhep.2016.05.022.

[6] X. Wang, Y. Hua, G. Xu, S. Deng, D. Yang, X. Gao, Targeting EZH2 for glioma therapy with a novel nanoparticle–siRNA complex, Int. J. Nanomed. 14 (2019) 2637–2653, https://doi.org/10.2147/IJN.S189871.

[7] Y. Wu, J. Hu, H. Ding, L. Chen, Y. Zhang, R. Liu, P. Xu, D. Du, W. Lu, J. Liu, Y. Liu, Y.-C. Liu, J. Lu, J. Zhang, Z. Yao, C. Luo, Identification of novel EZH2 inhibitors through pharmacophore-based virtual screening and biological assays, Bioorg. Med. Chem. Lett 26 (2016) 3813–3817, https://doi.org/10.1016/j.bmcl.2016.05.018.

[8] J. Antonio Asensio, E.M. Sánchez, P. Gómez-Romero, Proton -conducting membranes based on benzimidazole polymers for high-temperature PEM fuel cells . A chemical quest, Chem. Soc. Rev. 39 (2010) 3210–3239, https://doi.org/10.1039/B922650H.

[9] N. Sridhar Goud, P. Kumar, R. Dawn Bharath, Recent developments of target-based benzimidazole derivatives as potential anticancer agents, in: Heterocycles - Synthesis and Biological Activities, IntechOpen, 2020, https://doi.org/10.5772/intechopen.90758.

[10] A.V. Kabanov, H.E. Gendelman, Nanomedicine in the diagnosis and therapy of neurodegenerative disorders, Prog. Polym. Sci. 32 (2007) 1054–1082, https://doi.org/10.1016/j.progpolymsci.2007.05.014.

[11] N. Mody, R. Sharma, S.P. Vyas, Assessment of release kinetics of Docetaxel loaded PLGA nanoparticles, Asian J. Pharm. Pharmacol. 5 (2019) 1031–1037, https://doi.org/10.31024/ajpp.2019.5.5.24.

[12] K. Thanki, R.P. Gangwal, A.T. Sangamwar, S. Jain, Oral delivery of anticancer drugs: challenges and opportunities, J. Contr. Release 170 (2013) 15–40, https://doi.org/10.1016/j.jconrel.2013.04.020.

[13] R.M. Mainardes, M.P.D. Gremião, Nanoencapsulation and characterization of zidovudine on poly(L-lactide) and poly(L-lactide)—poly(ethylene glycol)-blend nanoparticles. https://doi.org/10.1166/jnn.2012.6638, 2012.

[14] R.K. Averineni, G.V. Shavi, A.K. Gurram, P.B. Deshpande, K. Arumugam, N. Maliyakkal, S.R. Meka, U. Nayanabhirama, PLGA 50:50 nanoparticles of paclitaxel: development, in vitro anti-tumor activity in BT-549 cells and in vivo evaluation, Bull. Mater. Sci. 35 (2012) 319–326, https://doi.org/10.1007/s12034-012-0313-7.

[15] C. Altmeyer, T.K. Karam, N.M. Khalil, R.M. Mainardes, Tamoxifen-loaded poly(L-lactide) nanoparticles: development, characterization and in vitro evaluation of cytotoxicity, Mater. Sci. Eng. C 60 (2016) 135–142, https://doi.org/10.1016/j.msec.2015.11.019.

[16] H.K. Makadia, S.J. Siegel, Poly lactic-co-glycolic acid (PLGA) as biodegradable controlled drug delivery carrier, Polymers 3 (2011) 1377–1397, https://doi.org/10.3390/polym3031377.

[17] L. Li, C. Li, J. Zhou, Effective sustained release of 5-FU-loaded PLGA implant for improving therapeutic index of 5-FU in colon tumor, Int. J. Pharm. 550 (2018) 380–387, https://doi.org/10.1016/j.ijpharm.2018.07.045.

[18] K. Anwer, M. Mohammad, E. Ezzeldin, F. Fatima, A. Alalaiwe, M. Iqbal, Preparation of sustained release apremilast-loaded PLGA nanoparticles: in vitro characterization and in vivo pharmacokinetic study in rats, IJN 14 (2019) 1587–1595, https://doi.org/10.2147/IJN.S195048.

[19] S.K. Knutson, T.J. Wigle, N.M. Warholic, C.J. Sneeringer, C.J. Allain, C.R. Klaus, J. D. Sacks, A. Raimondi, C.R. Majer, J. Song, M.P. Scott, L. Jin, J.J. Smith, E. J. Olhava, R. Chesworth, M.P. Moyer, V.M. Richon, R.A. Copeland, H. Keilhack, R. M. Pollock, K.W. Kuntz, A selective inhibitor of EZH2 blocks H3K27 methylation and kills mutant lymphoma cells, Nat. Chem. Biol. 8 (2012) 890–896, https://doi.org/10.1038/nchembio.1084.

[20] A.R. Jesus, M.R.C. Soromenho, L.R. Raposo, J.M.S.S. Esperança, P.V. Baptista, A. R. Fernandes, P.M. Reis, Enhancement of water solubility of poorly water-soluble drugs by new biocompatible N-acetyl amino acid N-alkyl cholinium-based ionic liquids, Eur. J. Pharm. Biopharm. 137 (2019) 227–232, https://doi.org/10.1016/j.ejpb.2019.03.004.

[21] A. Daina, O. Michielin, V. Zoete, SwissADME: a free web tool to evaluate pharmacokinetics, drug-likeness and medicinal chemistry friendliness of small molecules, Sci. Rep. 7 (2017) 1–12, https://doi.org/10.1038/srep42717.

[22] S.S. Katiyar, E. Muntimadugu, T.A. Rafeeqi, A.J. Domb, W. Khan, Co-delivery of rapamycin- and piperine-loaded polymeric nanoparticles for breast cancer treatment, Drug Deliv. (2015) 1–9, https://doi.org/10.3109/10717544.2015.1039667.

[23] E. Ramadan, T. Borg, G.M. Abdelghani, N.M. Saleh, Transdermal microneedle-mediated delivery of polymeric lamivudine-loaded nanoparticles, J. Pharmaceut. Technol. Drug Res. 5 (2016) 1, https://doi.org/10.7243/2050-120X-5-1.

[24] M.M. Silva, R. Calado, J. Marto, A. Bettencourt, A.J. Almeida, L. Gonçalves, Chitosan nanoparticles as a mucoadhesive drug delivery system for ocular administration, Mar. Drugs 15 (2017) 370.

[25] Singh, Preparation, characterization, and in vitro release study of albendazole-encapsulated nanosize liposomes, IJN (2010) 101, https://doi.org/10.2147/IJN.S8030.

[26] T. Higuchi, Rate of release of medicaments from ointment bases containing drugs in suspension, J. Pharmaceut. Sci. 50 (1961) 874–875.

[27] N.A. Peppas, Analysis of Fickian and non-Fickian drug release from polymers, Pharm. Acta Helv. 60 (1984) 110–111.
[28] P. Costa, J.M.S. Lobo, Modeling and comparison of dissolution profiles, Eur. J. Pharmaceut. Sci. 13 (2001) 123–133.
[29] R. Klasco, D.I. USP, Drug Information for the Health Care Provider, United States Pharmacopeial Convention, 2004.
[30] C.A.S. Bergström, P. Larsson, Computational prediction of drug solubility in water-based systems: qualitative and quantitative approaches used in the current drug discovery and development setting, Int. J. Pharm. 540 (2018) 185–193, https://doi.org/10.1016/j.ijpharm.2018.01.044.
[31] C.A.S. Bergström, W.N. Charman, C.J.H. Porter, Computational prediction of formulation strategies for beyond-rule-of-5 compounds, Adv. Drug Deliv. Rev. 101 (2016) 6–21, https://doi.org/10.1016/j.addr.2016.02.005.
[32] C.L. Stoner, M.D. Troutman, C.E. Laverty, Pharmacokinetics and ADME optimization in drug discovery, in: S. Neidle (Ed.), Cancer Drug Design and Discovery, Elsevier, New York, 2011, p. 31.
[33] Y. Ran, N. Jain, S.H. Yalkowsky, Prediction of aqueous solubility of organic compounds by the general solubility equation (GSE), J. Chem. Inf. Comput. Sci. 41 (2001) 1208–1217, https://doi.org/10.1021/ci010287z.
[34] K. Edueng, D. Mahlin, C.A.S. Bergström, The need for restructuring the disordered science of amorphous drug formulations, Pharm. Res. (N. Y.) 34 (2017) 1754–1772, https://doi.org/10.1007/s11095-017-2174-7.
[35] M. Morgen, C. Bloom, R. Beyerinck, A. Bello, W. Song, K. Wilkinson, R. Steenwyk, S. Shamblin, Polymeric nanoparticles for increased oral bioavailability and rapid absorption using celecoxib as a model of a low-solubility, high-permeability drug, Pharm. Res. (N. Y.) 29 (2012) 427–440, https://doi.org/10.1007/s11095-011-0558-7.
[36] B.C. Hancock, M. Parks, What is the true solubility advantage for amorphous pharmaceuticals? Pharm. Res. (N. Y.) 17 (2000) 397–404, https://doi.org/10.1023/A:1007516718048.
[37] R.M. Mainardes, M.P.D. Gremião, R.C. Evangelista, Thermoanalytical study of praziquantel-loaded PLGA nanoparticles, Rev. Bras. Ciencias Farm. 42 (2006) 523–530, https://doi.org/10.1590/S1516-93322006000400007.
[38] U.C. Oz, B. Küçüktürkmen, B. Devrim, O.M. Saka, A. Bozkir, Development and optimization of alendronate sodium loaded PLGA nanoparticles by central composite design, Macromol. Res. 27 (2019) 857–866, https://doi.org/10.1007/s13233-019-7119-z.
[39] N. Tahir, A. Madni, A. Correia, M. Rehman, V. Balasubramanian, M.M. Khan, H. A. Santos, Lipid-polymer hybrid nanoparticles for controlled delivery of hydrophilic and lipophilic doxorubicin for breast cancer therapy, IJN 14 (2019) 4961–4974, https://doi.org/10.2147/IJN.S209325.
[40] M. Mehanny, R.M. Hathout, A.S. Geneidi, S. Mansour, Studying the effect of physically-adsorbed coating polymers on the cytotoxic activity of optimized bisdemethoxycurcumin loaded-PLGA nanoparticles, J. Biomed. Mater. Res. 105 (2017) 1433–1445, https://doi.org/10.1002/jbm.a.36028.
[41] J.P. Rao, K.E. Geckeler, Polymer nanoparticles: preparation techniques and size-control parameters, Prog. Polym. Sci. 36 (2011) 887–913, https://doi.org/10.1016/j.progpolymsci.2011.01.001.
[42] S. Schubert, J. Joseph, T. Delaney, U.S. Schubert, Nanoprecipitation and nanoformulation of polymers : from history to powerful possibilities beyond poly (lactic acid), Soft Matter 7 (2011) 1581–1588, https://doi.org/10.1039/C0SM00862A.
[43] R. Dinarvand, S.H. Moghadam, A. Sheikhi, F. Atyabi, Effect of surfactant HLB and different formulation variables on the properties of poly-D,L-lactide microspheres of naltrexone prepared by double emulsion technique, J. Microencapsul. 22 (2005) 139–151, https://doi.org/10.1080/02652040400026392.
[44] R. Lopes, C.V. Eleutério, L.M.D. Gonçalves, M.E.M. Cruz, A.J. Almeida, Lipid nanoparticles containing oryzalin for the treatment of leishmaniasis, Eur. J. Pharmaceut. Sci. 45 (2012) 442–450, https://doi.org/10.1016/j.ejps.2011.09.017.
[45] P. Rafiei, A. Haddadi, Docetaxel-loaded PLGA and PLGA-PEG nanoparticles for intravenous application: pharmacokinetics and biodistribution profile, Int. J. Nanomed. 12 (2017) 935–947, https://doi.org/10.2147/IJN.S121881.
[46] B.B.S. Cerqueira, A. Lasham, A.N. Shelling, R. Al-Kassas, Development of biodegradable PLGA nanoparticles surface engineered with hyaluronic acid for targeted delivery of paclitaxel to triple negative breast cancer cells, Mater. Sci. Eng. C 76 (2017) 593–600, https://doi.org/10.1016/j.msec.2017.03.121.
[47] I. Brigger, C. Dubernet, P. Couvreur, Nanoparticles in cancer therapy and diagnosis, Adv. Drug Deliv. Rev. 54 (2002) 631–651, https://doi.org/10.1016/S0169-409X(02)00044-3.
[48] F. Yuan, M. Dellian, D. Fukumura, M. Leunig, D.A. Berk, V.P. Torchilin, R.K. Jain, Vascular permeability in a human tumor xenograft: molecular size dependence and cutoff size, Canc. Res. 55 (1995) 3752–3756.
[49] P. Couvreur, C. Vauthier, Nanotechnology: intelligent design to treat complex disease, Pharm. Res. (N. Y.) 23 (2006) 1417–1450, https://doi.org/10.1007/s11095-006-0284-8.
[50] I.A. Abdel Raheem, A. Abdul Razek, A.A. Elgendy, N.M. Saleh, M.I. Shaaban, F. K. Abd El-Hady, Design, evaluation and antimicrobial activity of Egyptian propolis-loaded nanoparticles: intrinsic role as A novel and naturally based root canal nanosealer, Int. J. Nanomed. 14 (2019) 8379–8398, https://doi.org/10.2147/IJN.S219577.
[51] S. Honary, B. Hoseinzadeh, P. Shalchian, The effect of polymer molecular weight on citrate crosslinked chitosan films for site-specific delivery of a non-polar drug, Trop. J. Pharmaceut. Res. 9 (2010) 525–531.
[52] S.-B. Sun, P. Liu, F.-M. Shao, Q.-L. Miao, Formulation and evaluation of PLGA nanoparticles loaded capecitabine for prostate cancer, Int. J. Clin. Exp. Med. 8 (2015) 19670–19681.
[53] S. Acharya, S.K. Sahoo, PLGA nanoparticles containing various anticancer agents and tumour delivery by EPR effect, Adv. Drug Deliv. Rev. 63 (2011) 170–183, https://doi.org/10.1016/j.addr.2010.10.008.
[54] J.-W. Yoo, E. Chambers, S. Mitragotri, Factors that control the circulation time of nanoparticles in blood: challenges, solutions and future prospects. https://www.ingentaconnect.com/content/ben/cpd/2010/00000016/00000021/art00002, 2010. (Accessed 20 December 2019).
[55] S. Fredenberg, M. Wahlgren, M. Reslow, A. Axelsson, The mechanisms of drug release in poly(lactic-co-glycolic acid)-based drug delivery systems—a review, Int. J. Pharm. 415 (2011) 34–52, https://doi.org/10.1016/j.ijpharm.2011.05.049.
[56] B. Zhang, P.S. Lung, S. Zhao, Z. Chu, W. Chrzanowski, Q. Li, Shape dependent cytotoxicity of PLGA-PEG nanoparticles on human cells, Sci. Rep. 7 (2017) 1–8, https://doi.org/10.1038/s41598-017-07588-9.
[57] S.V. Jadhav, P.S. Shewale, B.C. Shin, M.P. Patil, G.D. Kim, A.A. Rokade, S.S. Park, R.A. Bohara, Y.S. Yu, Study of structural and magnetic properties and heat induction of gadolinium-substituted manganese zinc ferrite nanoparticles for in vitro magnetic fluid hyperthermia, J. Colloid Interface Sci. 541 (2019) 192–203, https://doi.org/10.1016/j.jcis.2019.01.063.
[58] S.S. Sahoo, C.B. Rao, A.K. Mehta, Formulation development and optimization of nanosuspension of simvastatin for improved solubility by nanomilling, J. PharmaSciTech 5 (2015) 78–86.
[59] M. Teixeira, M. Pedro, M.S.J. Nascimento, M.M.M. Pinto, C.M. Barbosa, Development and characterization of PLGA nanoparticles containing 1,3-dihydroxy-2-methylxanthone with improved antitumor activity on a human breast cancer cell line, Pharmaceut. Dev. Technol. 24 (2019) 1104–1114, https://doi.org/10.1080/10837450.2019.1638398.
[60] E. Ahnfelt, E. Sjögren, P. Hansson, H. Lennernäs, In vitro release mechanisms of doxorubicin from a clinical bead drug-delivery system, J. Pharmaceut. Sci. 105 (2016) 3387–3398, https://doi.org/10.1016/j.xphs.2016.08.011.
[61] G. Li, L. Cao, Z. Zhou, Z. Chen, Y. Huang, Y. Zhao, Rapamycin loaded magnetic Fe3O4/carboxymethylchitosan nanoparticles as tumor-targeted drug delivery system: synthesis and in vitro characterization, Colloids Surf. B Biointerfaces 128 (2015) 379–388, https://doi.org/10.1016/j.colsurfb.2015.02.035.
[62] R. Thaler, S. Spitzer, H. Karlic, K. Klaushofer, F. Varga, DMSO is a strong inducer of DNA hydroxymethylation in pre-osteoblastic MC3T3-E1 cells, Epigenetics 7 (2012) 635–651, https://doi.org/10.4161/epi.20163.
[63] S.L.-K. Au, C.C.-L. Wong, J.M.-F. Lee, D.N.-Y. Fan, F.H. Tsang, I.O.-L. Ng, C.-M. Wong, Enhancer of zeste homolog 2 epigenetically silences multiple tumor suppressor microRNAs to promote liver cancer metastasis, Hepatology 56 (2012) 622–631, https://doi.org/10.1002/hep.25679.
[64] T. Yamashita, A. Budhu, M. Forgues, X.W. Wang, Activation of hepatic stem cell marker EpCAM by Wnt–β-catenin signaling in hepatocellular carcinoma, Canc. Res. 67 (2007) 10831–10839, https://doi.org/10.1158/0008-5472.CAN-07-0908.
[65] E.-Y. Wang, S.-H. Yeh, T.-F. Tsai, H.-P. Huang, Y.-M. Jeng, W.-H. Lin, W.-C. Chen, K.-H. Yeh, P.-J. Chen, D.-S. Chen, Depletion of β-catenin from mature hepatocytes of mice promotes expansion of hepatic progenitor cells and tumor development, Proc. Natl. Acad. Sci. Unit. States Am. 108 (2011) 18384–18389, https://doi.org/10.1073/pnas.1116386108.
[66] J.-H. Sun, Q. Luo, L.-L. Liu, G.-B. Song, Liver cancer stem cell markers: progression and therapeutic implications, World J. Gastroenterol. 22 (2016) 3547, https://doi.org/10.3748/wjg.v22.i13.3547.